AD-A044 422 UNITED TECHNOLOGIES RESEARCH CENTER EAST HARTFORD CONN F/G 20/4
FREE-VORTEX AERODYNAMIC WINDOW LEAKAGE INVESTIGATION.(U)
AUG 77 M D KROSNEY, R N GUILE F44620-73-C-0031
UNCLASSIFIED UTRC/R77-912076-3 AFOSR-TR-77-1205 NL

1 OF 1
ADA
044422

END
DATE
FILMED
10-77
DDC

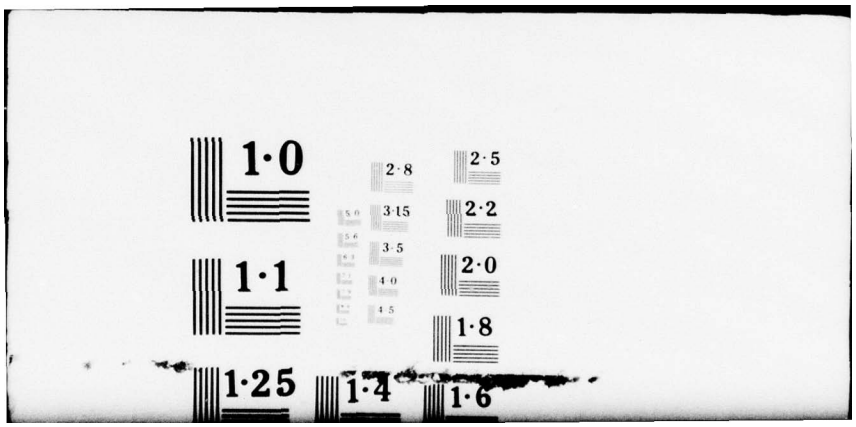
1·0
1·1
1·25
1·4
1·6
1·8
2·0
2·2
2·5
2·8
3·15
3·5
4·0
4·5
5·0
5·6

AFOSR-TR- 77-1205

(12)

UNITED TECHNOLOGIES RESEARCH CENTER

AIR FORCE OFFICE OF SCIENTIFIC RESEARCH (AFSC)
NOTICE OF TRANSMITTAL TO DDC
This technical report has been reviewed and is approved for public release IAW AFR 190-12 (7b).
Distribution is unlimited.
A. D. BLOSE
Technical Information Officer

SECURITY CLASSIFICATION OF THIS PAGE (When Data Entered)

REPORT DOCUMENTATION PAGE

READ INSTRUCTIONS BEFORE COMPLETING FORM

1. REPORT NUMBER: AFOSR-TR-77-1205	2. GOVT ACCESSION NO.
3. RECIPIENT'S CATALOG NUMBER	
4. TITLE (and Subtitle): FREE-VORTEX AERODYNAMIC WINDOW LEAKAGE INVESTIGATION	5. TYPE OF REPORT & PERIOD COVERED: FINAL, 1 Jan 73 — 30 June 1977
6. PERFORMING ORG. REPORT NUMBER: UTRC/R77-912076-3	
7. AUTHOR(s): M. D. KROSNEY, R. N. GUILE	8. CONTRACT OR GRANT NUMBER(s): F44620-73-C-0031
9. PERFORMING ORGANIZATION NAME AND ADDRESS: UNITED TECHNOLOGIES RESEARCH CENTER, 400 MAIN STREET, EAST HARTFORD, CONNECTICUT 06108	10. PROGRAM ELEMENT, PROJECT, TASK AREA & WORK UNIT NUMBERS: 2307A3, 61102F
11. CONTROLLING OFFICE NAME AND ADDRESS: AIR FORCE OFFICE OF SCIENTIFIC RESEARCH/NA, BLDG 410, BOLLING AIR FORCE BASE, D C 20332	12. REPORT DATE: Aug 77
	13. NUMBER OF PAGES: 64
14. MONITORING AGENCY NAME & ADDRESS (if different from Controlling Office)	15. SECURITY CLASS. (of this report): UNCLASSIFIED
	15a. DECLASSIFICATION DOWNGRADING SCHEDULE

16. DISTRIBUTION STATEMENT (of this Report)

Approved for public release; distribution unlimited.

17. DISTRIBUTION STATEMENT (of the abstract entered in Block 20, if different from Report)

18. SUPPLEMENTARY NOTES

19. KEY WORDS (Continue on reverse side if necessary and identify by block number)

AERODYNAMIC WINDOW
BOUNDARY LAYERS
FLOW VISUALIZATION

20. ABSTRACT (Continue on reverse side if necessary and identify by block number)

An experimental program was conducted to investigate the source of the leakage across a free-vortex aerodynamic window and to examine methods of reducing this leakage. Characterization of the endwall boundary layer flow via flow visualization techniques and pitot pressure measurements shows that the endwall boundary layer flow is deflected toward the free-vortex center and portions of it are ingested into the simulated laser cavity connecting duct. Passive boundary layer control by means of a base region, circumferential to the simulated laser cavity connecting duct aperture along the free-vortex inner boundary, decreased

DD FORM 1 JAN 73 1473 EDITION OF 1 NOV 65 IS OBSOLETE

UNCLASSIFIED

SECURITY CLASSIFICATION OF THIS PAGE (When Data Entered)

the minimum connecting duct pressure obtainable from 71 to 46 torr by reducing the amount of endwall boundary layer flow that was ingested by the connecting duct. Active boundary layer control via energization with high velocity air also reduced leakage into the connecting duct; but, because of deleterious interactions of the boundary layer flow with the nozzles used to inject the energization flow, no net improvement in the value of the ambient-to-cavity pressure ratio over the passive boundary layer control technique was obtained. Also, it was demonstrated that the free-vortex aerodynamic window can be used to exhaust purge gas flow from the simulated laser cavity connecting duct without severely compromising its performance as an aerodynamic window.

UNITED TECHNOLOGIES RESEARCH CENTER

UNITED TECHNOLOGIES

East Hartford, Connecticut 06108

(12)

R77-912076-3

Free-Vortex Aerodynamic Window Leakage Investigation

Prepared for:

Department of the Air Force
Air Force Office of Scientific Research (AFSC)
Bolling Air Force Base, D. C. 20332

Prepared by: Mark Kroovey

Prepared by: Eugene Gibb

APPROVED BY Roy Delmas

DATE August 1977

NO. OF PAGES _____

COPY NO. 3

FOREWORD

In 1973 the United Technologies Research Center undertook a study of aerodynamic window performance and optical quality under Air Force Office of Scientific Research Contract F44620-73-C-0031. During the first year of the contract performance period (i.e., from January 1, 1973 through December 31, 1973) a multi-stream analytical procedure was developed to compute a flow field downstream from a nozzle array such as would be used in a multi-element free-vortex aerodynamic window. A computer code was assembled based on this procedure and was used to calculate the flow field for an existing aerodynamic window device. The flow field results were used to calculate the effect of the aerodynamic window flow on a 10.6 μm laser beam. The predicted aerodynamic features and the estimated effect of the flow on the laser beam were in general agreement with existing experimental results. Also during this initial contract period, a portion of the effort was devoted to a survey of existing techniques for predicting the effect of turbulence on a laser beam. The results of the above investigation are reported in AFOSR-TR-74-1283, "Aerodynamic Window Performance and Optical Quality" by R. J. Flaherty, E. A. Kush and R. N. Guile. A users manual for the multi-stream computer code is contained in AFOSR-TR-74-1282, "A Multi-Stream Compressible Flow Computerized Analysis" by R. J. Flaherty.

The research effort for the period January 1, 1974 through December 31, 1975 was centered on an investigation of the interaction of a laser beam with a turbulent shear flow. The effects having the potential for causing laser beam degradation were assessed and general approaches to the analysis of the influence of these effects on the laser beam were reviewed. A model representing the turbulent eddies within the shear layer as discrete spheres which perturb the laser phase profile was formulated. Experiments were performed to measure the mean square phase fluctuations within a visible wavelength probe laser beam transmitted through a turbulent shear flow. These measurements, made using a UTRC-developed wide-bandwidth phase measurement technique, showed phase fluctuations in excess of one radian at visible wavelengths. When the fluctuations were scaled inversely with wavelength to 10.6 μm, the estimated decrease in peak far-field intensity was found to be approximately two percent. This work is reported in AFOSR-TR-75-0615, "Effect of a Turbulent Shear Flow on a Laser Beam" by E. A. Kush, S. N. Mapes and H. T. Couch.

The work reported herein was a continuation of the investigation of aerodynamic window performance and optical quality. An investigation of the interaction between aerodynamic window endwall boundary layers and leakage past the aerodynamic window was begun in 1975. This investigation was pursued during the period January 1, 1976 to June 30, 1977. Dr. Roy N. Guile was the Principal Investigator during this time period, and he and Mr. Mark D. Krosney directed the technical effort. Scientific management and support from AFSC was provided by Mr. Paul A. Thurston, Program Manager, Directorate of Aerospace Sciences.

Free-Vortex Aerodynamic Window Leakage Investigation

TABLE OF CONTENTS

SUMMARY

An experimental program was conducted to investigate the source of the leakage across a free-vortex aerodynamic window and to examine methods of reducing this leakage. Characterization of the endwall boundary layer flow via flow visualization techniques and pitot pressure measurements shows that the endwall boundary layer flow is deflected toward the free-vortex center and portions of it are ingested into the simulated laser cavity connecting duct. Passive boundary layer control by means of a base region, circumferential to the simulated laser cavity connecting duct aperture along the free-vortex inner boundary, decreased the minimum connecting duct pressure obtainable from 71 to 46 torr by reducing the amount of endwall boundary layer flow that was ingested by the connecting duct. Active boundary layer control via energization with high velocity air also reduced leakage into the connecting duct; but, because of deleterious interactions of the boundary layer flow with the nozzles used to inject the energization flow, no net improvement in the value of the ambient-to-cavity pressure ratio over the passive boundary layer control technique was obtained. Also, it was demonstrated that the free-vortex aerodynamic window can be used to exhaust purge gas flow from the simulated laser cavity connecting duct without severely compromising its performance as an aerodynamic window.

INTRODUCTION

The aerodynamic window provides a means for extracting the output laser beam from high-power laser cavities in which the high optical flux levels prohibit the use of solid windows. In the absence of a solid window, the pressure difference between the laser cavity and the atmosphere is supported by the change in momentum of the supersonic aerodynamic window flow which seals the otherwise open port. For laser cavities operating at subatmospheric pressures, this seal prevents disturbance of the laser cavity by ingestion of atmospheric gases. In evaluating the performance of the aerodynamic window, the primary areas of concern are: (1) the amount of mass flow required by the aerodynamic window to produce the desired momentum change, (2) the ability of the aerodynamic window to transmit the laser beam with minimum optical quality degradation, and (3) the effectiveness of the aerodynamic window in preventing or controlling leakage of ambient gases into the laser cavity.

Exploratory tests wherein water was injected into the endwall region of an aerodynamic window flow indicated the leakage past the aerodynamic window to be associated with the endwall boundary layers. Accordingly, the present investigation was undertaken to explore the interrelation between the endwall boundary layers and the leakage characteristics of the aerodynamic window. The experimental effort included flow visualization of the endwall boundary layer flow, pitot pressure surveys in the endwall region, evaluation of alternative aperture configurations designed to reduce leakage flow, the exploration of the use of endwall boundary energization to reduce leakage and determination of the capability of the aerodynamic window to aspirate flow from the duct connecting it to the laser cavity.

BACKGROUND AND STATEMENT OF THE PROBLEM

Application of an aerodynamic window is illustrated in Fig. 1. In this example the aerodynamic window utilizes a nozzle which delivers a uniform supersonic flow at its exit. The momentum change required to support the pressure difference between the surroundings and the low pressure laser cavity is accomplished by turning the nozzle effluent through an expansion fan (Refs. 1, 2). The momentum change may also be produced using an oblique shock (Ref. 3) or combinations of expansions and oblique shocks (Refs. 4 through 7) downstream of the nozzle exit.

In designing efficient laser systems it is desirable to minimize the amount of flow needed to drive the aerodynamic window. For a given pressure difference between the laser and the surroundings, the momentum change of the aerodynamic window jet is fixed, thus the vector change in jet velocity must be maximized if the aerodynamic window flow requirements are to be minimized. Assuming the magnitude of the jet velocity to be unchanged in flowing over the aperture, it follows that the amount of flow turning experienced by the aerodynamic window jet must be maximized. The amount of flow turning attained with aerodynamic windows employing uniform-flow supply nozzles is usually limited by the strengths of the shocks and expansions and by the requirement for efficient exhaust of the aerodynamic window flow. The free-vortex aerodynamic window of Fig. 2 (Ref. 8) utilizes a supply nozzle which provides a nonuniform supersonic jet well suited to large amounts of flow turning. The flow issuing from this nozzle is characterized by a free-vortex velocity distribution wherein the flow velocity varies inversely with the radius of curvature of the jet at the nozzle exit.

A cross-section of a full 360 deg free vortex with its circular arc streamlines is shown in Fig. 3a. The limiting radii, R_o and R_∞, where the local velocity ratios, V/a^*, correspond to unity and infinite Mach number, respectively, are indicated. The aerodynamic window (Fig. 2) utilizes that segment of the free vortex (Fig. 3b) bounded by the inner and outer radii R_1 and R_2 and included within the flow turning angle, $\Delta\theta$. The width of the segment normal to the plane of Figs. 2 and 3 is fixed by the width of the aperture to be sealed. By selecting the velocity, a^*, and the total pressure, P_{TAW}, in combination with the free-vortex velocity and pressure distributions (Fig. 3c) the static pressures at R_1 and R_2 can be matched to the laser cavity and ambient pressures (P_L and P_{AMB}), respectively. With the flow conditions matched in this manner, the flow over the aperture is turned gradually by the Mach lines of the supersonic flow. Since the flow turning is maintained by the Mach waves present at the nozzle exit, strong shock waves are avoided, thereby offering the potential for increased flow turning and reduced supply requirements.

The original application of the free-vortex aerodynamic window concept employed a multi-element nozzle to approximate the supersonic free-vortex flow (Refs. 9, 10). The free-vortex velocity distribution (Fig. 3c) was approximated

by a stepped profile produced by a stacked array of supersonic nozzles. Each element of the array produced a flow differing in Mach number and static pressure from the flow issuing from the adjacent element. The flow mismatch between adjacent elements resulted in a series of shock waves and expansion fans distributed through the flow.

The initial effort under the present contract was centered on the analysis of the multi-element approximation to the free-vortex aerodynamic window. A computerized analysis was developed to calculate flow fields typical of multi-element free-vortex aerodynamic windows. The analysis predicts the flow boundaries, location and strength of shocks and expansions, and the variation in refractive index due to inviscid effects within the flow. The analysis was applied to compute the flow field and calculate the optical distortion for the aerodynamic window device of Refs. 9 and 10. A description of the analysis and the results of the calculations are presented in Ref. 11. A User's Manual describing the input/output information for the computerized code is contained in Ref. 12.

In practice, the aerodynamic window flow is not fully represented by its inviscid properties alone. Instead, free shear layers exist at the boundaries of the flow (R_1 and R_2 in Fig. 2). The optical distortion due to turbulence within these shear layers is not taken into account in an inviscid analysis. The effect of these shear layers on the optical properties of a laser beam was the subject of a second investigation under this contract. A discrete-sphere turbulence model, formulated to account for the interaction of the laser beam with shear layer eddies, is described in Ref. 13. Also described in Ref. 13 are the results of experiments in which a wide-band phase measurement technique was used to measure near-field mean square phase fluctuations in a shear layer.

The most recently completed effort under this investigation was directed towards the problem of leakage of gases past the aerodynamic window into the laser cavity. Such leakage reduces the effectiveness of the seal provided by the aerodynamic window. In many applications the leakage past the aerodynamic window is used to purge the duct connecting the aerodynamic window to the laser cavity, thereby eliminating potentially stagnant gas zones in the beam path. However, because laser operation can be deleteriously affected by this leakage (e.g., the laser diffuser performance may be degraded by leakage of low momentum flow into the laser flow), it is important to be able to control the leakage. In other applications (Ref. 14), a negative leakage (a flow from the connecting duct out through the aerodynamic window) may be desired. The ability to support a negative leakage requires not only elimination of the leakage from the aerodynamic window into the laser, but also aspiration of the flow from the connecting duct by the aerodynamic window.

As discussed above, the pressure difference across the aperture between the atmosphere and a low pressure laser cavity is supported by a change in momentum of the aerodynamic window stream. If it is assumed that the magnitude of the average velocity is unchanged as the aerodynamic window stream crosses the aperture,

the momentum change is the result of the change in stream direction only. (Referring to Figs. 2 and 3, the streamlines of the free-vortex aerodynamic window flow are lines of constant Mach number, thus the momentum change is solely dependent on the change in flow direction.) The velocities in the boundary layer flow on the aerodynamic window endwalls (the walls parallel to the plane of the paper in Fig. 2) are lower than in the inviscid core flow. If the boundary layer flow were to experience the same degree of flow turning as the core flow, the momentum change would be less and the ability of the boundary layer flow to support the pressure difference between the atmosphere and the laser cavity would be reduced. The consequence of the reduced pressure support capability is the establishment of a cross flow in the boundary layer region. This leakage flow allows gases which may have moisture or other contaminants deleterious to optimum laser power extraction into the laser cavity. Also this leakage flow must be removed from the cavity via the diffuser used to exhaust the laser cavity flow. The performance of these devices is typically limited to a prescribed operating envelope and the addition of low Mach number leakage flow represents a situation which adversely affects the diffuser operation.

EXPERIMENTAL PROGRAM

An experimental program was conducted to determine if cross flow in the endwall boundary layer of a free-vortex aerodynamic window was the source of leakage into the laser cavity connecting duct, and to explore methods of reducing this leakage. Flow visualization via ink injection into the boundary layer and pitot pressure measurements were used to characterize the boundary layer flow. Two methods of boundary layer control, one passive and one active, were investigated to reduce leakage into the connecting duct. The potential of the free-vortex aerodynamic window to exhaust flow from the connecting duct was also investigated.

Test Equipment and Operational Procedures

Aerodynamic Window Model

The aerodynamic window model shown in Fig. 4 consists of the supply nozzle located upstream of the laser beam path, an aperture region centered on the laser beam path, and a diffuser section having inner and outer diffuser walls downstream from the laser beam path. The laser beam path extends from the laser cavity through the aerodynamic window into the surroundings. The model is nominally sized for a square 3.80-cm aperture.

The flow direction in Fig. 4 is from left to right. The nozzle exit plane is inclined at a 30-deg angle to the laser beam path which in turn is inclined at 30 deg to the inner diffuser wall. The air supply is introduced to the nozzle plenum through a 1.91-cm port, then expanded through the nozzle having a 0.287 x 3.80-cm throat to develop the free-vortex velocity distribution, and exhausts at the nozzle exit plane. The design nozzle exit plane static pressure on the laser cavity side is 1/15 atm while on the atmospheric side the pressure is 1.0 atm. The flow starts its arcuate path at the nozzle exit plane and turns through an angle of 60 deg as it spans the aperture. After sealing the aperture, the flow enters the diffuser and is decelerated to atmospheric pressure. Note that the inner diffuser wall is set back 0.508 cm from the location of the circular arc (dot-dash line) which constitutes the inner boundary of the ideal free-vortex segment. This provides space for growth of the jet resulting from its mixing with the gas in the aperture.

The cross section of the aperture that the laser beam path passes through can be changed from a 3.80-cm square to a 3.49-cm dia circle or to a 3.11-cm dia circle by the insertion of appropriate filler blocks into the 3.80-cm square aperture. The filler blocks (shown in Fig. 4) are secured in place with set screws. The surface of the filler blocks adjacent to the aerodynamic window flow is parallel to the arcuate path described by the free vortex flow from the aerodynamic window nozzle. This surface blends tangentially with the inner diffuser wall. Reducing the cross section of the aperture by use of the filler blocks introduces a base region around the simulated laser cavity connecting duct.

Atmospheric air is entrained along the outer jet boundary and ingested into the diffuser. The outer diffuser wall is designed so that its leading edge lies on a line extended from the downstream edge of the aperture and parallel with the laser beam path as indicated in phantom on Fig. 4. A diffuser inlet height of 3.96 cm, measured along this line, was used during this program. The aerodynamic window aperture is connected to a vacuum pump for the removal of any leakage past the aerodynamic window.

The model was fabricated using aluminum, brass and lucite. The nozzle contour blocks are free-machining brass while the plenum block is aluminum. The plenum end plates, base piece, and inner and outer diffuser walls are aluminum; the endwalls are lucite to permit flow visualization experiments. All other parts are aluminum. The model was sealed with 'O' ring material and pourable silicone rubber in appropriate areas.

The analytical design of the free-vortex aerodynamic window used in this study is documented in Ref. 8; the model itself is the property of UTRC.

Test Facility

The free-vortex aerodynamic test model was installed in the UTRC Gas Dynamic Laboratory on the Stand 24A airflow centerline. This installation is shown in Fig. 5. The airflow for the aerodynamic window nozzle was supplied by a 400-psi (27.2-atm) air supply system which is capable of delivering dry air at flow rates up to 4.5 kg/sec. The pressure of the filtered airflow at the aerodynamic window nozzle was adjusted by means of a hand operated throttling valve. A 12.9-atm rupture disc located downstream of the throttling valve prevented overpressuring of the model. The aerodynamic window supply air and atmospheric air entrained by the window flow were exhausted through a 35.5-cm dia duct to the atmosphere. Air from a 1000-psi (68-atm) air supply system was used to supply flow to the endwall boundary layer energizers when necessary. Flow was exhausted from the simulated laser cavity connecting duct via a line to the Stokes vacuum system.

Instrumentation and Data Recording Equipment

The pressures in the nozzle supply plenum and in the simulated laser cavity connecting duct were measured with a 0-200 psia and a 0-100 torr Wallace and Tiernan Bourdon tube type pressure gauge, respectively. The flowrate of the gases exhausted from the laser cavity connecting duct was computed using data acquired from a 0-100 torr and 0-50 torr Wallace and Tiernan Bourdon tube pressure gauge sensing the upstream and the throat pressures, respectively, of a 2.54-cm dia ASME long radius flow meter. All data were manually recorded.

General Test Procedures

The free-vortex aerodynamic window is designed to operate at an ambient-to-cavity pressure ratio of 15 at an aerodynamic window supply pressure of 10 atm and a flow rate of 0.264 kg/sec. The pressure support characteristic for the aerodynamic window was established by determining the ambient-to-cavity pressure ratio over a range of aerodynamic window supply pressures. Figure 6 shows pressure support data for the free-vortex aerodynamic window with a 3.49-cm dia circular aperture installed at the simulated laser cavity connecting duct. Also shown in Fig. 6 is the envelope of the pressure support characteristic established for the 3.49-cm aperture; performance outside this envelope indicated some problem with the aerodynamic window, such as a nozzle seal leak or a leak in an instrumentation line. Different pressure support characteristics were obtained for different apertures. The pressure support characteristic for each configuration was routinely determined to ensure no problems had developed with the model.

Test procedures specific to each of the various phases of the experimental program are described within the appropriate section of this report.

Flow Visualization Experiments

Leakage across an aerodynamic window can be deleterious to laser operation. This leakage manifests itself as a flow across the endwall boundary layer. In order to be able to control or eliminate this leakage flow some insight regarding the behavior of the flow adjacent to the endwall must be obtained. The observation of the flow patterns generated via ink injection in the endwall boundary layer regions was used to gain this insight. Tests were conducted with three different apertures: (1) a 3.80-cm square aperture, (2) a 3.49-cm diameter circular aperture and (3) a 3.11-cm circular aperture. The base regions of the circular apertures were intended to divert the cross flow in the endwall boundary layer, thereby providing passive boundary layer control, in an attempt to reduce leakage past the aerodynamic window and improve the pressure support characteristics of the device.

Test Technique

Several methods of obtaining visible traces of the boundary layer flow on the lucite endwalls of the free-vortex aerodynamic window model were evaluated. Initially India ink was injected into the endwall boundary layer through a probe having a hypodermic tip. Next the India ink was injected into the endwall boundary layer through a series of small holes drilled in the endwall, both along the nozzle exit plane and on the laser beam axis. The major problem encountered in both techniques was the difficulty in controlling the amount and rate of India ink injection. Consequently, it was very difficult to prevent splattering of the ink or agglomeration of dried ink at the injection site. After testing a number of different injectants, it was found that a mixture of fast drying strip chart ink and methanol could be used without the splattering or agglomeration problems encountered with India ink. This injectant mixture provided a successful means to obtaining well-defined flow patterns on the lucite endwall. The injectant used consisted of Hewlett-Packard 1530-0706 ink mixed with methanol in one-to-one proportions. In these proportions, the mixture formed a uniform liquid sheet when poured over lucite or glass and did not agglomerate on the endwalls. The ink/methanol mixture was injected using a 0.0635-cm diameter needle affixed to a one-cubic-centimeter B-D tuberculin syringe.

Flow visualization tests were typically conducted in the following manner. After the aerodynamic nozzle flow was established at the desired condition, the tip of the syringe was positioned near the inside of the lucite endwall and a small quantity of the ink/methanol mixture was discharged from the syringe. The syringe tip was then moved to another location and the process was repeated until the flow pattern on the endwall in the region of interest was defined. The application of this technique is illustrated in the photograph of Fig. 7. This technique was difficult to use, however, in the proximity of the nozzle exit plane because of problems involved in positioning the syringe tip in the high-speed flow while simultaneously injecting the ink. Instead, the flow patterns at the nozzle exit plane were defined by first "preloading" several drops of ink along the endwall at the nozzle exit plane prior to initiating the aerodynamic window flow. The flow patterns were then constructed by rapidly opening the supply valve to establish the desired flow condition.

The particle paths defined by the ink on the endwalls were illuminated with a photoflood light and photographed using Polaroid Type 52 black and white film at a shutter speed of 1/125 sec at an aperture setting of f/22.

Flow visualization tests, for selected configurations, conducted with the ink mixture injected on both endwalls showed no difference between the flow patterns generated on either endwall. Also, the majority of the flow visualization tests were conducted at the nozzle design supply pressure of 10 atm. The results of tests conducted at a supply pressure of 11.0 atm showed no qualitative differences in the flow patterns associated with the use of the higher supply pressure.

Test Results

3.80-cm Square Cross-Section Aperture

Photographs of the endwall flow patterns for the 3.80-cm square aperture without and with cavity leakage removal are shown in Fig. 8. The ink/methanol mixture was injected at the endwall in the area above the outer ideal free-vortex boundary. The flow pattern shown in Fig. 8a (zero cavity leakage removal) indicates that the flow along the endwall is deflected toward the inner ideal free-vortex boundary. That is, the curvature of the endwall flow pattern is greater than the curvature of the free-vortex flow emanating from the aerodynamic window nozzle as previously determined by shadowgraphic and schlieren flow visualization techniques (Ref. 8).

The endwall flow pattern shown in Fig. 8b reveals that with cavity leakage removal and concomitant reduction in cavity pressure the deflection of the flow along the endwall toward the center of the free-vortex is more pronounced. Whereas, in the absence of leakage removal, the endwall flow originating from above the aerodynamic window nozzle flow just catches the downstream corner of the aperture, with leakage removal, a large fraction of this flow is deflected down into the connecting duct towards the simulated laser cavity. A large recirculation pattern is visible in Fig. 8b on the endwall below the inner boundary of the ideal free-vortex.

Schematic representations of these flow patterns are shown in Figs. 9 and 10. The figures are constructed from data accumulated both from numerous photographs and from real time observations of flow patterns on the endwalls. Indicated in these figures are the flow patterns of (1) the adjacent atmospheric airflow, (2) the airflow in the strong mixing region between the atmospheric air and aerodynamic window nozzle flow, and (3) airflow from the aerodynamic window nozzle. The salient features of the flow patterns with zero leakage flow removal (see Fig. 9) are that (1) the flow along the endwall originating from the aerodynamic window nozzle is deflected toward the center of the vortex and all but that near the outer ideal free-vortex boundary is deflected into the duct connecting the aerodynamic window to the simulated laser cavity, (2) some of the atmospheric air flow from the mixing region is also deflected into the duct, and (3) the mixing region extends up to the outer diffuser wall.

Removing the cavity leakage flow (see Fig. 10) reduces the simulated laser cavity pressure from $\sim$ 75 torr down to $\sim$ 25 torr, and a more severe deflection of the endwall flow toward the center of the vortex is noted. All of the endwall flow originating from within the nozzle and a much larger portion of the airflow in the mixing region are turned down into the connecting duct adjoining the simulated laser cavity. The airflow into the duct forms a recirculation pattern along the endwall, a pattern which was only suggested in the zero leakage removal case. (Although a recirculation pattern is not evident on the endwall in the zero leakage removal case of Fig. 9, recirculation must exist in the zero leakage removal case in order to conserve mass.) With cavity leakage removal, the mixing region does

not meet the top diffuser wall within the region under observation. This suggests that, with leakage removal, a greater quantity of atmospheric air enters the diffuser through the wider space between the intense mixing region and the diffuser wall.

3.49-cm Circular Cross-Section Aperture

A 3.49-cm dia hole was machined into a 3.80-cm square aluminum filler block to form a new aperture for the aerodynamic window (cf. Fig. 4). The surface of the aperture block had the same curvature as the inner free-vortex boundary and blended tangentially into the bottom diffuser wall. The difference in cross-sectional area between a 3.80-cm square and a 3.49-cm dia circle formed a base region around the circular aperture as shown in Fig. 4. This base region, in effect, provides passive boundary layer control by diverting the endwall boundary layer cross flow away from the connecting duct.

Photographs of the endwall flow pattern for the 3.49-cm dia circular cross-section aperture without and with cavity leakage removal are shown in Fig. 11. Here, as in Fig. 8, the flow along the endwalls is deflected toward the vortex center with the more pronounced deflection occurring for the case with cavity leakage removal where the simulated laser cavity pressure is reduced from $\sim$ 50 torr to $\sim$ 15 torr. However, with this circular aperture, the endwall flow does not appear to turn into the simulated laser cavity but instead is diverted downstream into the diffuser by the base area formed by the filler block.

Figures 12 and 13 show schematic representations of the flow patterns for the 3.49-cm circular aperture without and with cavity leakage flow removal, respectively. As shown in Fig. 12, the endwall flow originating from the aerodynamic window nozzle is deflected toward the free-vortex center due to the pressure differential existing between the atmospheric side and the simulated laser cavity side. In contrast to the pattern of Fig. 9 obtained with the 3.80-cm square aperture, the flow appears to be turned downstream toward the diffuser by the base formed by the filler block. The same pattern is apparent in the portion of the endwall flow originating in the mixing region. Nevertheless, it was noted during these tests (as indicated by the ink traces) that some of the airflow from the nozzle and the mixing region did indeed flow across the base of the aperture and into the connecting duct near the laser beam axis ($\Delta\theta$ = 30 deg). With cavity leakage removal (see Fig. 13) the deflection of the airflow toward the simulated laser cavity is more pronounced. This suggests that the pressure in the base region formed by the filler block is lower with leakage removal than without leakage removal. Thus, although the base region formed by the filler block succeeds in diverting some of the cross flow away from the connecting duct, a portion of the cross flow does enter the connecting duct causing a leakage into the simulated laser cavity.

The diversion of the cross flow effected by the base region between the circular and square apertures reduces the leakage of endwall boundary layer flow past the aerodynamic window into the simulated laser cavity. The reduced leakage also improves the pressure support characteristics of the aerodynamic window, allowing the device to operate with zero leakage removal at lower cavity pressures.

The effect on the pressure support characteristic (of the free-vortex aerodynamic window) of reducing endwall cross flow leakage by using the circular aperture configuration is shown in Fig. 14. At the 10-atm design supply pressure, use of the 3.49-cm dia circular aperture filler block, which provides a base region 0.124-cm wide at its minimum cross section, increased the pressure support ratio to 14.5 compared to the ratio of 10.2 obtained using the 3.80-cm square aperture. The peak pressure support ratio, occurring at a 10.8-atm supply pressure, was similarly increased from 11.8 to 17.2 through the use of the filler block.

3.11-cm Circular Cross-Section Aperture

The flow visualization patterns obtained with the 3.11-cm diameter circular cross-section aperture were similar in character to those obtained with the 3.49-cm circular aperture. The nozzle airflow and airflow from the mixing region are deflected toward the vortex center and are turned back toward the diffuser along the aperture base. The deflection of the endwall airflow is greater with cavity leakage than without, but it is difficult to discern any differences between flow visualization photographs obtained for the two circular apertures. Results obtained with a circular aperture having a 3.11-cm diameter show a slightly improved support characteristic when compared to the results for the 3.49-cm diameter aperture at supply pressures beloe 10.4 atm (see Fig. 14).

Summary of Flow Visualization Results

The results of the flow visualization tests indicate that the flow patterns in the endwall boundary layer are strongly influenced by cavity leakage flow removal. The removal of this cavity leakage flow, which reduces the simulated laser cavity pressure, results in a more pronounced deflection of the endwall flow toward the center of the ideal free-vortex because of the increased pressure gradient across the endwall boundary layer. Furthermore, the use of an aperture insert which provides a base area, or boundary layer fence, is an effective method of turning a large fraction of the deflected endwall flow downstream into the diffuser thereby reducing leakage flow into the simulated laser cavity and increasing the pressure support characteristics of the aerodynamic window. Increasing the width of the base region from 0.124 cm to 0.305 cm by reducing the aperture diameter from 3.49 cm to 3.11 cm did not significantly alter the flow visualization or pressure support data. However, alternative aperture configurations should be further investigated to fully develop this means of passive boundary layer control as an effective technique to reduce cavity leakage flow.

Pitot Pressure Profile Measurements

Pitot pressure measurements were obtained close to the endwalls to characterize the boundary layer flow and verify that it is a source of leakage into the simulated laser cavity connecting duct. Free stream pitot pressure measurements were obtained at the nozzle exit plane and compared with theoretical predictions derived from isentropic flow relations for an ideal gas. Free stream pitot pressure measurements were also obtained at two locations downstream of the nozzle exit plane to determine if the flow field from the aerodynamic window maintained a free-vortex pitot pressure profile.

Test Technique and Equipment

Pitot pressure profiles were mapped along radial lines at various positions (z) away from the endwall at each of three angular positions ($\Delta\theta$ = 0, 30 and 60 deg, where the nozzle exit plane lies along $\Delta\theta$ = 0) in the coordinate system of the ideal free-vortex as illustrated in Fig. 2. Measurements were obtained with two different aperture configurations: 1) a 3.80-cm square cross-section aperture and a 3.49-cm dia circular cross-section aperture. Furthermore, each configuration was tested with and without cavity leakage removal from the simulated laser cavity connecting duct.

The pitot measurements were made with a probe which consists of a series of stainless steel hypodermic tubes silver soldered within tubes of large diameter (shown in Fig. 15a). The probe tip was formed by a piece of 0.089-cm diameter by 0.01-cm wall hypodermic tube which was flattened so as to be 0.053 cm in the z direction (minor axis) and 0.112 cm in the r direction (major axis).

The probe was mounted in a motorized mechanism (see Fig. 15b) which enabled the probe to be traversed in a radial direction. The spacing between the probe tip and the endwall, z, was established by inserting gauge blocks between the probe tip and the endwall and fixing the probe in the mount. The data were obtained at 13 values of z ranging from 0.0279 cm to 1.316 cm. Three different probe mounting blocks were used to orient the probe assembly at $\Delta\theta$ = 0-, 30- and 60-deg angular positions. The radial position of the probe was recorded on a Texas instrument X-Y plotter by means of a Bourns linear potentiometer with appropriate excitation and signal conditioning equipment. The pitot pressure measurement was recorded on the same X-Y plotter utilizing a 0-200 psia Statham strain gauge transducer with appropriate electronics. The probe was traversed from the minimum radial position to the maximum radial position, which required one minute, held stationary for approximately one minute, and then traversed back to the minimum radial position to ensure the validity and repeatability of the profile measurements.

Test Results

Representative profiles obtained at the nozzle exit plane ($\Delta\theta$ = 0 deg) for several values of z are shown in Fig. 16. Traces representing the pressure profiles are arranged in order from left to right for decreasing values of z. The general decrease in pitot pressure with decreasing radial position is not associated with boundary layer flow and is expected for this type of free-vortex aerodynamic window. The endwall boundary layer manifests itself by the general decrease in pressure with decreasing z position.

Free Stream Pitot Pressure Profiles

Free stream pitot pressure profiles (out of the influence of the endwalls) were obtained at angular positions of $\Delta\theta$ = 0, 30 and 60 deg for the 3.80-cm square cross section aperture and for the 3.49-cm dia circular cross section aperture without and with cavity leakage removal. Figure 17 shows a free stream pitot pressure normalized by the aerodynamic window supply pressure for the 3.49-cm dia aperture at $\Delta\theta$ = 0 deg (nozzle exit plane) with no cavity leakage removal. The decrease in pitot pressure with decreasing radial location as exhibited in Fig. 17 is associated with the increase in Mach number towards the center of the free-vortex generated by the aerodynamic window nozzle flow and agrees well with the theoretically predicted free stream pressure profile. The measured pitot pressure profile deviates from the theoretically predicted pressure profile at radial positions greater than r = 4.6 cm and less than r = 3.8 cm due to boundary layer flow along the inner and outer nozzle contours, and due to the size of the probe tip which allows pitot pressure outside the boundaries of the flow field of the nozzle to be "averaged" with the measurement obtained inside the flow field near the radial boundary. At an angular position $\Delta\theta$ = 30 degrees, as shown in Fig. 18, a character similar to the theoretical pressure profile presented in Fig. 17 is obtained but the regions where the measured pitot profile differs from the theoretical are now more extensive due to pressure losses associated with the mixing of the aerodynamic window nozzle flow with entrained atmospheric flow on the outer side of the aerodynamic window nozzle and with flow being entrained from the simulated laser cavity connecting duct on the inner side of the aerodynamic window nozzle. Figure 19 shows a profile for the 3.49-cm dia circular cross-section aperture at an angular position of $\Delta\theta$ = 60 degrees. The regions over which the pitot pressure measurements do not conform to the theoretical predicted values are now even more extensive, indicating further mixing losses along the outer and inner boundaries.

To permit the pitot pressures to be obtained at the $\Delta\theta$ = 60-deg angular position, a slot was cut in the top diffuser wall. The slot was 0.794 wide in the flow direction and extended 1.78 cm from one of the endwalls. The centerline of the slot was 2.14 cm from the leading edge of the outer diffuser wall. It was

initially thought that this slot would have little effect on the aerodynamic window performance, but its presence resulted in a measured cavity pressure of approximately 100 torr instead of the nominal 50 torr. The atmospheric flow through the slot caused a disturbance in the aerodynamic window flow field which partially blocked the flow channel and diverted some free stream flow toward the simulated laser cavity connecting duct increasing the duct pressure. The effect the flow through the slot had on the pitot pressure measurements at $\Delta\theta$ = 60 deg is not known quantitatively, but the qualitative effects were clearly stated. In all other tests the slot was sealed.

Free stream pitot pressure data were also obtained with leakage flow being removed from the simulated laser cavity connecting duct at a rate of $\dot{W}_L$ = 1.6 gm/sec. The removal of this leakage flow results in a decrease in the simulated laser cavity pressure, P_c, to nominally 15 torr from the 50 torr pressure level obtained with zero cavity leakage flow removed. The normalized free stream pitot pressure profile at $\Delta\theta$ = 0 is essentially unaffected by the removal of cavity leakage flow. However, at angular positions of $\Delta\theta$ = 30 and 60 degrees it can be seen that the inboard boundary of the pressure profile has moved closer to the center of the vortex (smaller r values) as seen in Figs. 20 and 21 (cf. Figs. 18 and 19). This is a result of the aerodynamic window nozzle flow expanding to match a pressure of 15 torr rather than 50 torr at the inboard boundary.

Free stream data for tests conducted with the 3.80-cm square cross section aperture show the same trends as seen with the 3.49-cm dia circular cross section aperture.

· Pitot Pressure Profiles in the Endwall Boundary Layers

The endwall boundary layer pitot pressure profiles are constructed by cross plotting the radial distributions, as shown in Fig. 16, obtained at various positions normal to the endwall. The endwall pitot pressure profiles shown in Fig. 22a were obtained for the 3.80-cm square cross section aperture at $\Delta\theta$ = 0 deg (nozzle exit plane) with and without leakage flow. At the radial positions of r = 4.01 cm, 4.52 cm and 4.78 cm it is seen that there is no sizable effect of cavity leakage flow on the aerodynamic window nozzle flow field at the nozzle exit plane. A slight reduction in pitot pressure is noted at r = 3.76 cm suggesting that the flow at the inner boundary of the vortex is expanding to the lower cavity pressure resulting from removing cavity leakage flow.

The data shown in Fig. 22b were obtained at an angular position $\Delta\theta$ = 30 deg (along the laser beam axis) with the 3.80-cm square aperture, with and without cavity leakage flow removal. At the radial position r = 3.76 cm with no cavity leakage removal, the low values of free stream pitot pressure indicate that the pitot probe was placed outside of the aerodynamic window nozzle flow field. The pitot pressure begins to increase at z $\cong$ 0.04 cm indicating that

there is flow near the endwall boundary. That is, it appears that flow has migrated towards the vortex center along the endwall. When the leakage flow is removed the values of pitot pressure are greater, indicating that the free stream is deflected towards the vortex center due to expansion to the lower cavity pressure along the inner vortex boundary, and the pitot probe is now immersed in the free stream flow. The pitot pressure in the attendant boundary layer is now lower than in the no leakage case because a portion of the boundary layer flow is being removed as cavity leakage flow. At a radial position of 4.01 cm the pitot pressure profiles normal to the endwall with and without cavity leakage are more similar. The free stream pitot pressure for the zero leakage condition is slightly higher than for the condition with leakage because the aerodynamic window nozzle flow had expanded toward the inner vortex boundary with leakage producing a lower peak pitot pressure. The pitot pressure in the endwall boundary layer for the case with leakage is lower than for the no leakage case for the same reason it was lower at r = 3.76 cm; that is, some of the boundary layer flow is being removed as cavity leakage flow. At increased values of r the effect of leakage removal is reduced until, at r = 4.8 cm, no effect is noted.

The pitot pressure profile data obtained at the angular location of $\Delta\theta$ = 60 deg for the 3.80-cm square aperture with and without cavity leakage flow removal are presented in Fig. 22c. These data show the same trends as observed at $\Delta\theta$ = 30 deg but here the effect of the entrained atmospheric flow at $\Delta\theta$ = 60 deg is evident from the relatively high level of pitot pressure well outside the ideal vortex boundary at r = 6.54 cm.

Pitot probe measurements with the 3.49-cm dia circular cross section aperture yielded data similar to the data obtained with the square aperture. For $\Delta\theta$ = 0 deg, shown in Fig. 23a, there is little effect of cavity leakage flow on the pitot pressure profiles. These data indicate that at the nozzle exit plane the reduced cavity pressure caused by cavity leakage removal only affects the pitot pressure at the inner vortex boundary. The data shown in Fig. 23b for angular position $\Delta\theta$ = 30 deg have the same characteristics as seen in Fig. 22b. Thickening of the boundary layer is evident at r = 3.63 cm. At an angular position $\Delta\theta$ = 60 deg the data presented in Fig. 23c exhibit the same traits as seen in Fig. 22C; that is: (1) low free stream pitot pressure at r = 3.76 cm and zero leakage removal with increasing pitot pressure at the endwall, (2) increased free stream pitot pressure with leakage removal at r = 3.76 cm, (3) a general shift toward the vortex inner boundary with leakage flow removal, and (4) increased pitot pressure outside of the vortex outer boundary due to atmospheric entrainment.

Summary of Pitot Profile Measurements

The pitot pressure profile data indicate that the endwall boundary layer flow turns inward toward the free-vortex center. Data obtained at angular positions of $\Delta\theta$ = 30 and 60 deg show that along the vortex inner boundary a larger pitot pressure is measured in the boundary layer than in the free stream. This result is observed for both the square and the circular apertures.

Endwall Boundary Layer Energization Tests

The pressure differential across the free-vortex aerodynamic window is supported by a momentum change in the aerodynamic window flow. Since the endwall boundary flow velocity is lower than the free-stream velocity, the atmospheric-to-cavity pressure differential causes increased turning in the boundary layer flow which leads to cross flow and subsequent leakage flow into the simulated laser cavity. A series of tests in which an attempt was made to energize the boundary layer by addition of high velocity along the endwalls was conducted.

Description of Configuration

Two nozzle arrays, one for each endwall, each consisting of four conical nozzles shown in Fig. 24 were designed to provide energization of the endwall boundary layer in the free-vortex aerodynamic window. Each conical nozzle had a 0.044-cm dia throat, a 15 deg half angle divergence, and an area ratio of 16. The installation of the energizers is shown schematically in Fig. 25. The endwall boundary layer energizers were designed so that the plane defined by the centerlines of the four conical nozzles was coincident with the surface of the endwalls adjacent to the aerodynamic window flow. To accommodate this energizer placement, a shallow truncated conical recess was machined into each lucite endwall. This conical recess provided a transition from the endwall to the energizer and back to the endwall with the energizer at various angular positions. The angular position, ϕ, of the energizer is defined as the angle measured in degrees between the laser beam path and the flow from the energizers. An 'O' ring was used to seal the energizer to the endwall.

The source of the energizer flow was the UTRC 1000 psi air supply system. Total energizer flow rates up to 0.066 kg/sec, or approximately 2.4 percent of the aerodynamic window flow were introduced through the energizers.

Test Results

Tests with No Energizer Flow

Tests were conducted with the 3.49-cm dia aperture at energizer angular positions of ϕ = 75, 90 and 105 deg. The pressure support characteristic for the free-vortex aerodynamic window with the energizer positioned at ϕ = 90 deg is shown in Fig. 26. The value of the ambient-to-cavity pressure ratio is lower than the value of the pressure ratio obtained without the energizers in the endwalls over the range of aerodynamic window nozzle supply pressures tested. The presence of the energizers apparently caused a flow disturbance along the endwall, which caused increased leakage into the simulated laser cavity connecting duct. The resultant ambient-to-cavity pressure ratio is lower than that obtained with the 3.80-cm square aperture seen in Fig. 14. With the energizers at angular positions of ϕ = 75 and 105 degrees, even smaller values of the ambient-to-cavity pressure ratio were obtained.

Test Results with Energizer Flow

Tests were conducted with the energizers at three angular positions, at energizer flow rates up to 2.4 percent of the aerodynamic window flow, and at aerodynamic window nozzle supply pressures from 9.5 to 11.9 atm. The effect of leakage flow removal on the simulated laser cavity connecting duct pressure was measured at several values of energizer flow. A cross plot of these data which shows the effect of energizer flow on leakage into the simulated laser cavity connecting duct is shown in Fig. 27. For a cavity pressure of 40 torr, for instance, the cavity leakage flow decreased from 5.07 gm/sec to 3.65 gm/sec (a 28 percent reduction) by increasing the energizer airflow from 0 to 2.4 percent of the aerodynamic window flow. Connecting duct pressures obtained for tests with the energizers at angular positions of ϕ = 75 and 105 deg were all greater than 95 torr.

Summary of Boundary Layer Energization Test Results

Results of the endwall boundary layer flow energization tests show that leakage into the simulated laser cavity connecting duct can be reduced by using high velocity flow to energize the endwall boundary layer. The test results also show that the aerodynamic window performance was adversely affected by the flow disturbances the energizers caused along the endwalls. These results indicate further investigation of active boundary layer control is warranted but care must be given to the design of the energizers to prevent the energizer configuration itself from causing increased leakage into the laser cavity connecting duct.

Entrainment of Purge Gases by the Aerodynamic Window

Typically, laser optics systems require that various components, such as mirrors, be purged with a clean inert gas to prevent optical quality degradation by the corrosive gases used in the laser system. Furthermore, the ducting which houses the various components of the laser optics train may require the use of purge gas to prevent reaction products from accumulating in the duct and absorbing laser power. A continuous flow of these purge gases must be provided. The continuous flow can be maintained by exhausting the purge gases through the laser cavity and attendant diffuser to the laser exhaust site. However, because the pressure recovery of the laser diffuser can be degraded by entrainment of large quantities of low Mach number purge flow, it would be desirable to use the aerodynamic window flow to remove the purge flow via entrainment. A limited number of tests were conducted to determine the feasibility of using the free-vortex aerodynamic window to exhaust purge flow from the connecting duct which joins the aerodynamic window to the simulated laser cavity.

Test Results and Discussion

Tests to determine the effect on cavity pressure of injecting various amounts of purge gas into the connecting duct between the aerodynamic window and the simulated laser cavity were conducted with the free-vortex aerodynamic window model. The purge gas was metered with a choked flow venturi and injected many connecting-duct diameters away from the aerodynamic window to ensure a uniform flow distribution at the interface between the aerodynamic window and the connecting duct. Tests were conducted at aerodynamic window nozzle supply pressures of 10, 11.1 and 11.6 atm using various flow rates of nitrogen or helium as the purge gas. The effect of purge gas mass flow on simulated laser cavity pressure is shown in Fig. 28a. As the amount of nitrogen added to the connecting duct was increased from 0 to 1.5 gm/sec, the cavity pressure increased from 53 torr to 98 torr for a nozzle supply pressure of 10 atm. Increasing the nozzle supply pressure did not appreciably change the resultant cavity pressures. When helium was used as the purge gas, a cavity pressure of 87 torr was obtained at a purge flow rate of 0.29 gm/sec. This pressure is considerably higher than that corresponding to an equivalent mass flow rate of nitrogen.

The rate at which a connecting duct of fixed geometry is cleansed by the purge gas, for a fixed cavity pressure, is proportional to the volumetric flow rate of the purge gas. Therefore, the effect of the purge gas on the performance of the aerodynamic window is better assessed relative to the volumetric flow rate of purge gas. When the pressure data of Fig. 28a are replotted in Fig. 28b versus volumetric flow rate, it is seen that the use of helium as a purge gas yielded a lower cavity pressure than nitrogen for an equivalent volumetric flow rate.

Thus, it has been demonstrated that a free-vortex aerodynamic window can be used to exhaust purge flow from the duct connecting the aerodynamic window to the simulated laser cavity. However, to exhaust the purge flow, the aerodynamic window must be capable of operating with little leakage at a simulated cavity pressure lower than the actual operating pressure of the laser cavity. The aerodynamic window tested under this program, for example, can be used to exhaust purge flow for lasers which operate at a cavity pressure of 50 torr or greater. Specifically the results of Fig. 32b show that the present aerodynamic window would be compatible with a laser system which operates at a cavity pressure of 70 torr and requires a purge gas flow rate of 30 liters/min. The capacity of the present aerodynamic window to exhaust purge gases would be increased by utilizing techniques which reduce or eliminate the leakage through the endwall boundary layers and hence allow the aerodynamic window to operate with zero leakage at a cavity pressure less than 50 torr.

CONCLUSIONS AND RECOMMENDATIONS

The results of experiments conducted under this program indicate that leakage across a free-vortex aerodynamic window is the result of cross flow in the endwall boundary layers. The flow patterns observed in flow visualization tests conducted without a net removal of flow from the simulated laser cavity clearly show that the endwall boundary layer flow is deflected toward the center of the ideal free-vortex and that a portion of the flow is ingested into the simulated laser cavity connecting duct. Furthermore, the tests reveal that a net removal of cavity leakage flow caused even more of the endwall boundary layer flow to be deflected into the simulated laser cavity connecting duct.

Evidence of cross flow in the endwall boundary layer was also observed in the results of the pitot pressure surveys. The pitot pressure measured at radial positions inside of the inner vortex boundary showed no free stream aerodynamic window flow but as the probe was moved closer to the endwall higher pitot pressures were observed. That is, the aerodynamic window flow had migrated radially toward the vortex inner boundary along the endwalls.

Flow visualization tests conducted with laser cavity connecting duct apertures with a base region at the endwalls indicated that the endwall boundary layer flow is diverted away from the laser cavity into the diffuser. Thus, the presence of base area between the laser cavity aperture and the endwall is a means of passive boundary layer control. Quantitatively, the pressure support characteristic for a configuration with an aperture having base area showed a 55 percent improvement in the ambient-to-cavity pressure ratio above that obtainable with an aperture configuration which does not provide a base region.

Another means of reducing the leakage into the simulated laser cavity is to energize the endwall boundary layer with high velocity airflow. This technique, an active boundary layer control technique, was used successfully in reducing the relative leakage across the aerodynamic window. However, the physical presence of the energizers used in this program, without energizer flow, distributed the endwall boundary layer flow and caused an increase in cavity leakage above that obtained through the passive boundary layer control method. With energizer flow the cavity leakage was reduced but not to the level obtained with the passive boundary layer control technique. Further design effort may achieve a net improvement with the active boundary layer control technique.

The ability of the free-vortex aerodynamic window to exhaust purge gases from the simulated laser cavity was demonstrated. However, to realize the full potential for exhausting purge gases through the aerodynamic window two factors must be

treated. First, the aerodynamic window must be designed so that the pressure at the interface with the laser cavity (vortex inner boundary) is lower than the operating cavity pressure of the attendant laser device. Second, to more easily achieve this design condition, the laser cavity leakage must be minimized or eliminated either by active or passive boundary layer control techniques.

Reduction of the leakage across the free-vortex aerodynamic window via passive boundary layer control mechanisms warrants further investigation to develop refined aperture configurations other than the initial configurations evaluated in this program. Also, boundary layer fences along the endwalls may lead to improved performance. This technique would utilize physical barriers to prevent inward migration of the boundary layer flow. Reduction of cavity leakage by energizing the endwall boundary layer flow also bears further investigation. Boundary layer flow energization by injecting high velocity flow parallel to the endwalls needs increased work. Based on the results of the limited testing conducted in this study, a great deal of care must be put in the design of the energizers so as not to deleteriously affect the flow along the endwalls and, thereby, negate the advantages of the technique. Another technique would employ an appropriate modification to the aerodynamic window nozzle contours to increase the momentum of the flow adjacent to the endwalls. This modification would be particularly attractive since it fully integrates the energizer with the aerodynamic window.

Finally, investigation of the aerodynamic interactions arising from integration of the aerodynamic window with the laser system should be pursued. Of particular interest are the effects of the purge system on the connecting duct flow patterns and possible acoustic interactions associated with coupling the aerodynamic window to a laser cavity.

REFERENCES

1. Hausmann, G. F.: Aerodynamic Window for Gas Dynamic Laser. United States Patent 3, 617, 928, United Aircraft Corporation, November 1971.

2. Zimet, E.: Aerodynamic Windows for Laser Beams. NOLTR 73-66, Naval Ordnance Laboratory, White Oak, Silver Spring, Md., March 1973.

3. Hausmann, G. F.: Aerodynamic Window. United States Patent 3, 654, 569, United Aircraft Corporation, April 1972.

4. Guile, R. N. and S. N. Mapes, Jr.: Aerodynamic Window Investigation. AFWL-TR-72-134, Air Force Weapons Laboratory, Albuquerque, New Mexico, October 1972.

5. Studerus, C. J., et al.: Investigation of Methods of Extracting a Laser Beam From a Gas Dynamic Laser. AFWL-TR-72-92, Air Force Weapons Laboratory, Albuquerque, New Mexico, May 1973.

6. Parmetier, E. M. and R. A. Greenberg: Supersonic Flow Aerodynamic Windows for High-Power Lasers. AIAA Journal, Vol. 11 No. 7, July 1973, pp. 943-949.

7. Jones, T. G.: Development of an Electric Discharge Laser Aerodynamic Window. AFWL-TR-73-105, Air Force Weapons Laboratory, Albuquerque, New Mexico, September 1973.

8. Guile, R. N. and W. E. Hilding: Investigation of a Free-Vortex Aerodynamic Window. AIAA Paper No. 75-122 presented at the AIAA 13th Aerospace Sciences Meeting, January 1975.

9. Coulter, L. J., R. N. Guile and M. N. Director: Aerodynamic Investigation of the Multi-Element Centrifugal Aerowindow. United Aircraft Research Laboratories Report UAR-M66, July 1973.

10. Guile, R. N., S. N. Mapes, Jr., M. N. Director and L. J. Coulter: Analysis and Testing of Full-Scale Aerodynamic Window. AFWL-TR-73-257, February 1974.

11. Flaherty, R. J., E. A. Kush and R. N. Guile: Aerodynamic Window Performance and Optical Quality. AFOSR-TR-74-1283, February 1974.

12. Flaherty, R. J.: A Multi-Stream Compressible Flow Computerized Analysis. AFOSR-TR-74-1282, May 1974.

REFERENCES (Cont'd)

13. Kush, E. A., S. N. Mapes and H. T. Couch: Effect of a Turbulent Shear Flow on a Laser Beam. AFOSR-TR-75-0615, February 1976.

14. Behrens, H. W., G. L. Grohs and C. L. Dailey: Aerodynamic Window for Chemical Laser. United States Patent 4, 013, 977, TRW, Inc., March 1977.

LIST OF SYMBOLS

a^*	Critical sound speed, m/sec
P_{AMB}	Local ambient pressure, torr
P_c	Simulated laser cavity connecting duct pressure, torr
P_p	Aerodynamic window flow field pitot pressure, psia
P_{TOW}	Aerodynamic window supply pressure, psia
$\dot{Q}_p$	Simulated purge volumetric flow rate, liters/min
r	Radial distance from the ideal free-vortex center, cm
R_1	Ideal free-vortex inner boundary, 3.76 cm in this study
R_2	Ideal free-vortex outer boundary, 4.76 cm in this study
R_L	Radius of nozzle inner wall, cm
Ru	Radius of nozzle outer wall, cm
Ro	Radius where $v/a^* = 1.0$, cm
R_∞	Radius corresponding to infinite Mach number for free vortex, cm
T_{TAW}	Aerodynamic window supply temperature, K
V	Magnitude of velocity vector, m/sec
$\dot{W}_{ENG}$	Normalized energizer mass flow rate, percent $\dot{W}_w$
$\dot{W}_L$	Cavity leakage removal mass flow rate, gm/sec
$\dot{W}_p$	Simulate purge mass flow rate, gm/sec
$\dot{W}_w$	Aerodynamic window nozzle mass flow rate, kg/sec
z	Distance perpendicular to end wall, cm

LIST OF SYMBOLS (Cont'd)

$\Delta\theta$	Angular position from nozzle exit plane, deg
ϕ	Relative angular position between laser beam axis and energizer flow angle, deg

AERODYNAMIC WINDOW

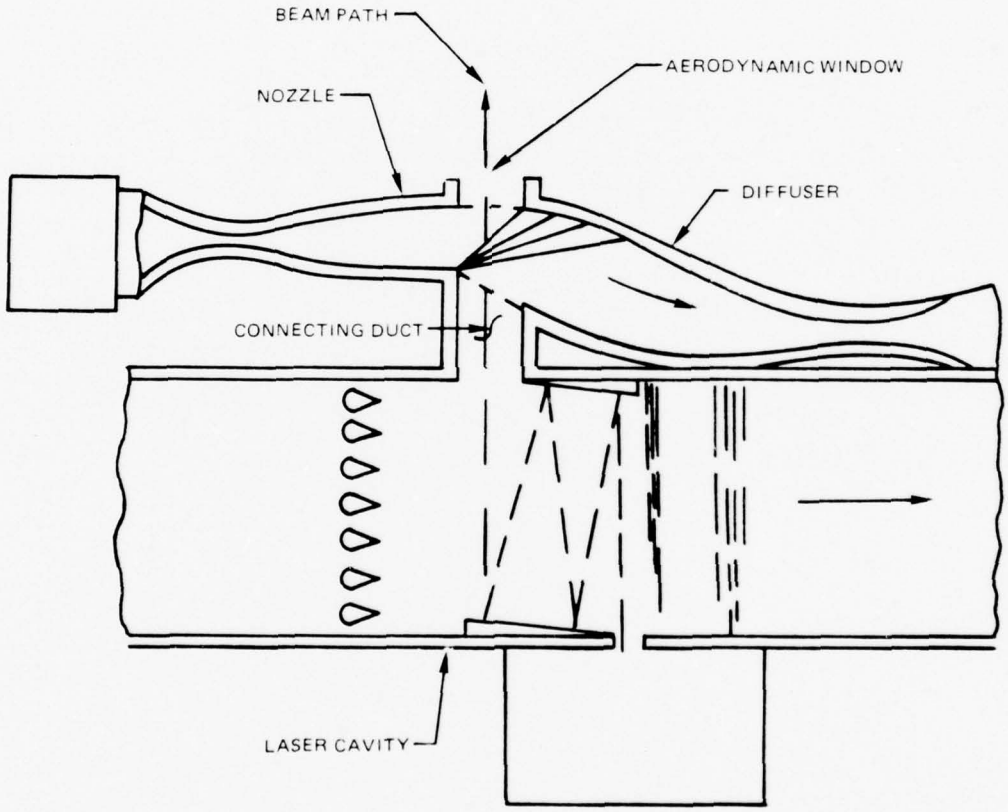

77-08-125-1

FIG. 2

FREE – VORTEX AERODYNAMIC WINDOW

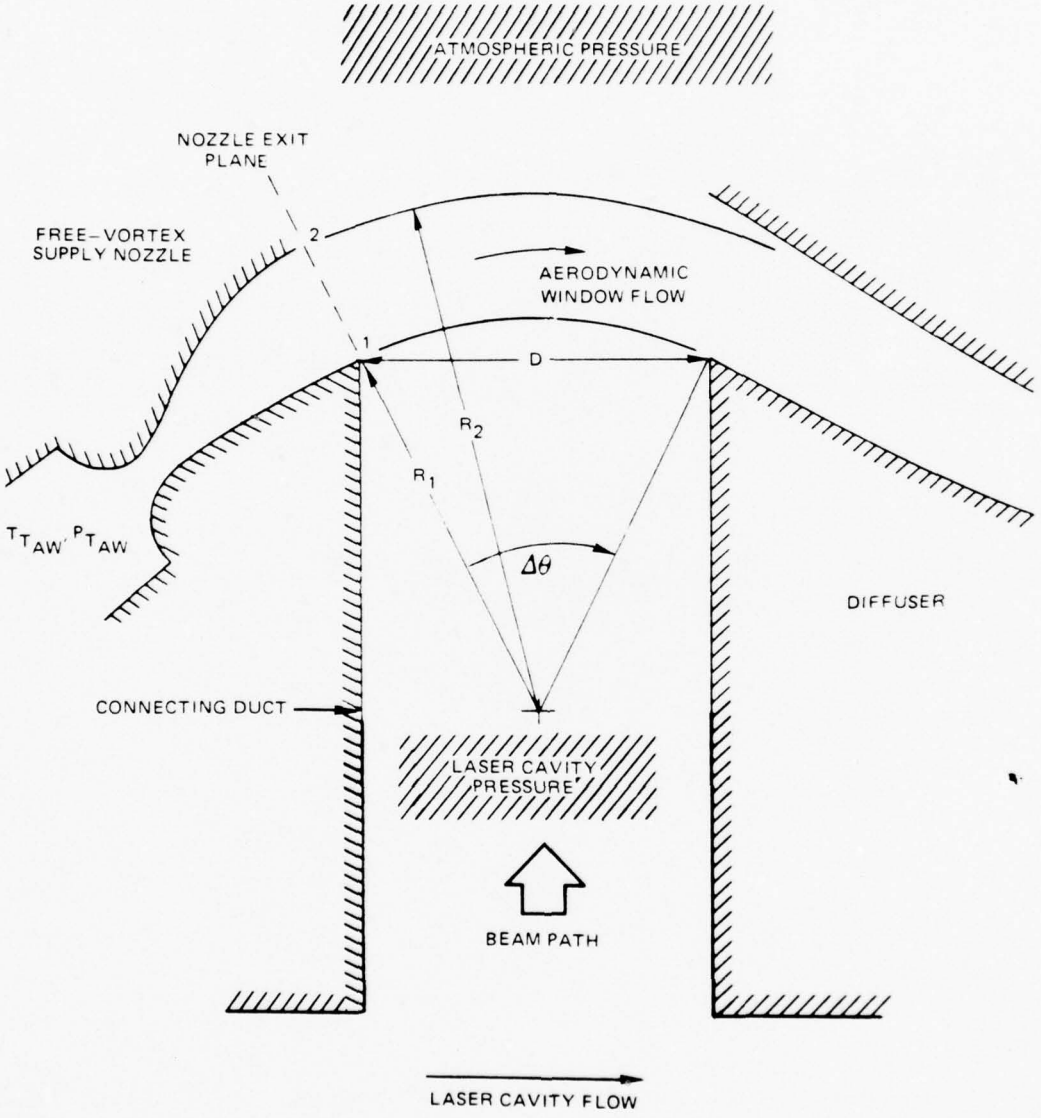

77-08-125-2

FREE - VORTEX FLOW FIELD

a. FREE-VORTEX STREAMLINES

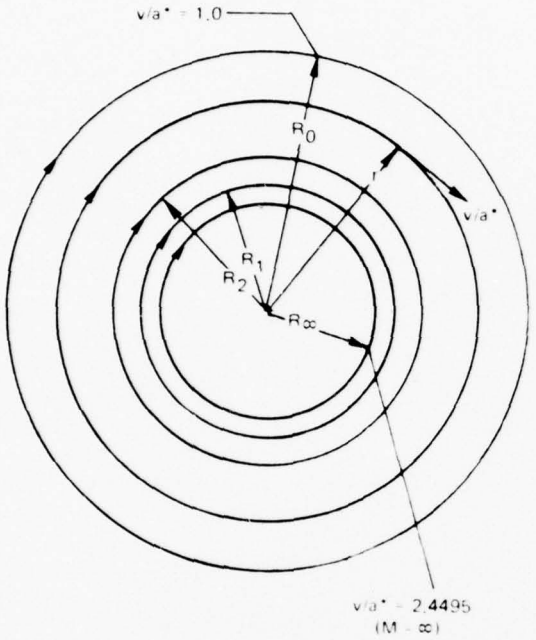

b. SEGMENT OF FREE-VORTEX

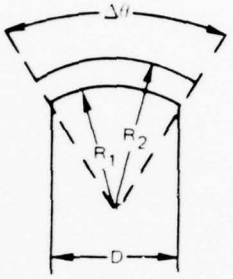

c. FREE-VORTEX FLOW PROPERTIES FOR $\gamma = 1.4$

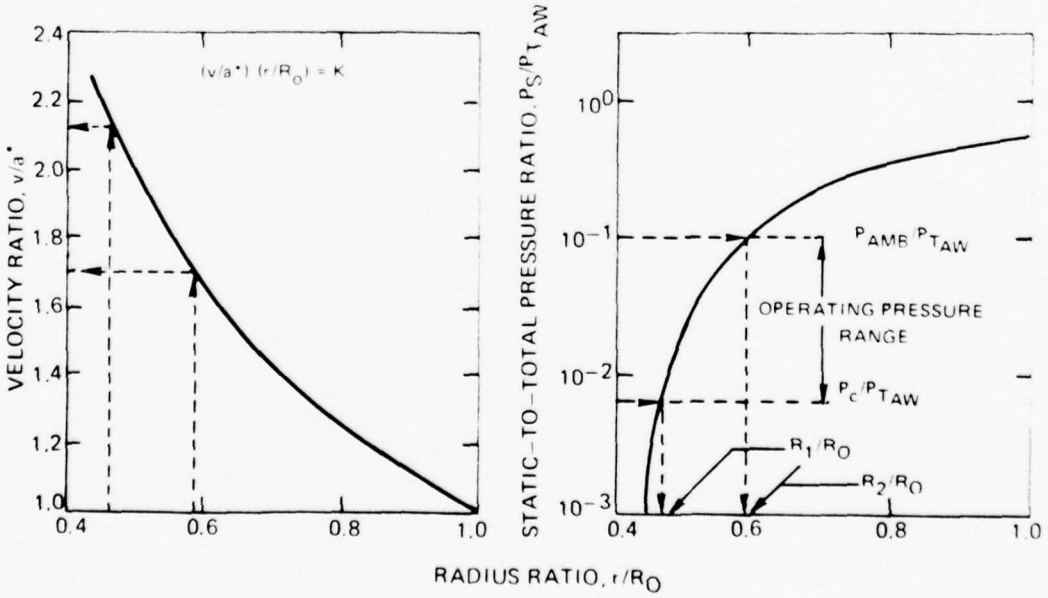

77-08-125-3

FREE–VORTEX AERODYNAMIC WINDOW MODEL

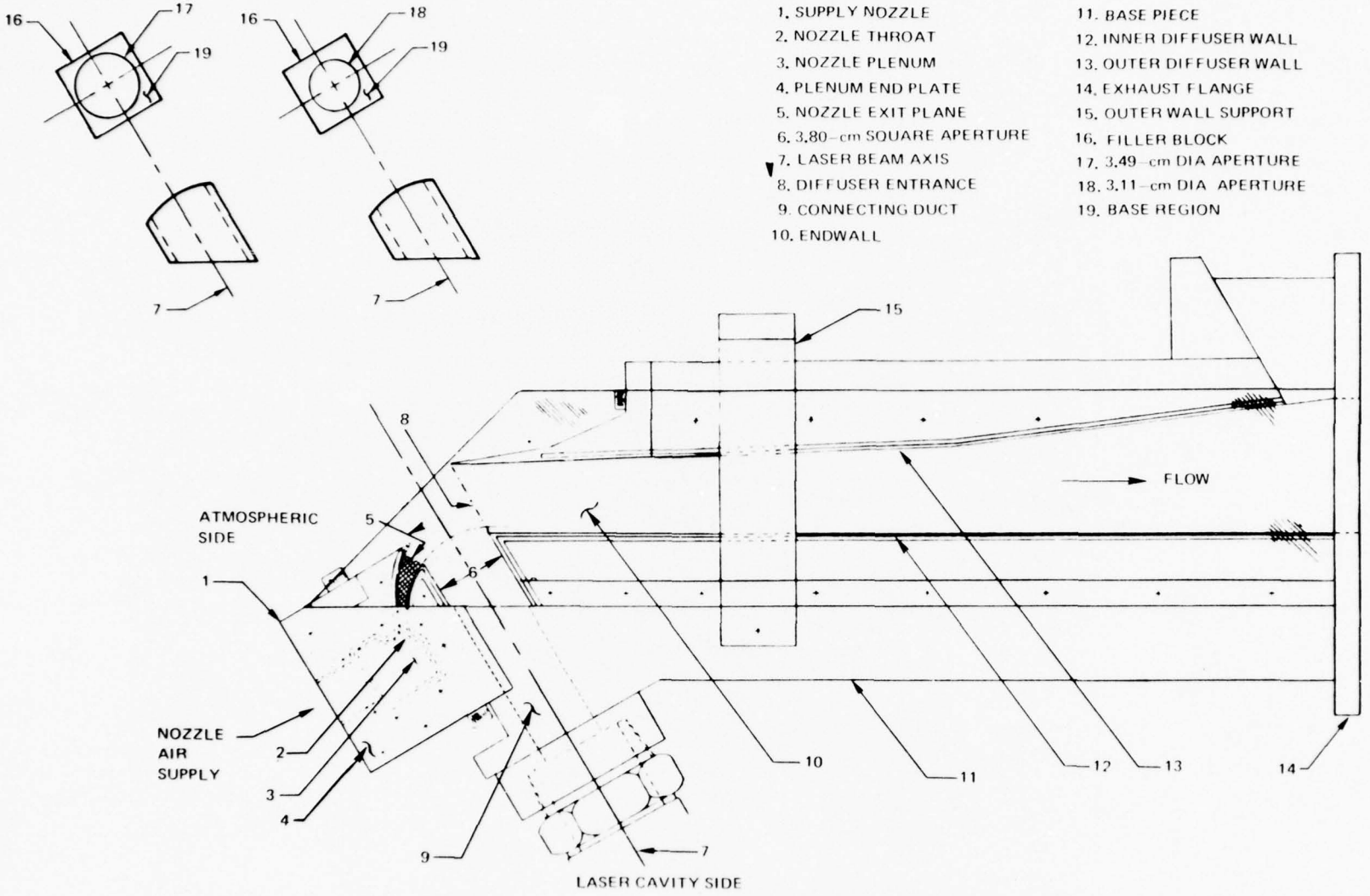

R77–912076–3

FIG. 4

FIG. 5

FREE VORTEX AERODYNAMIC WINDOW INSTALLATION

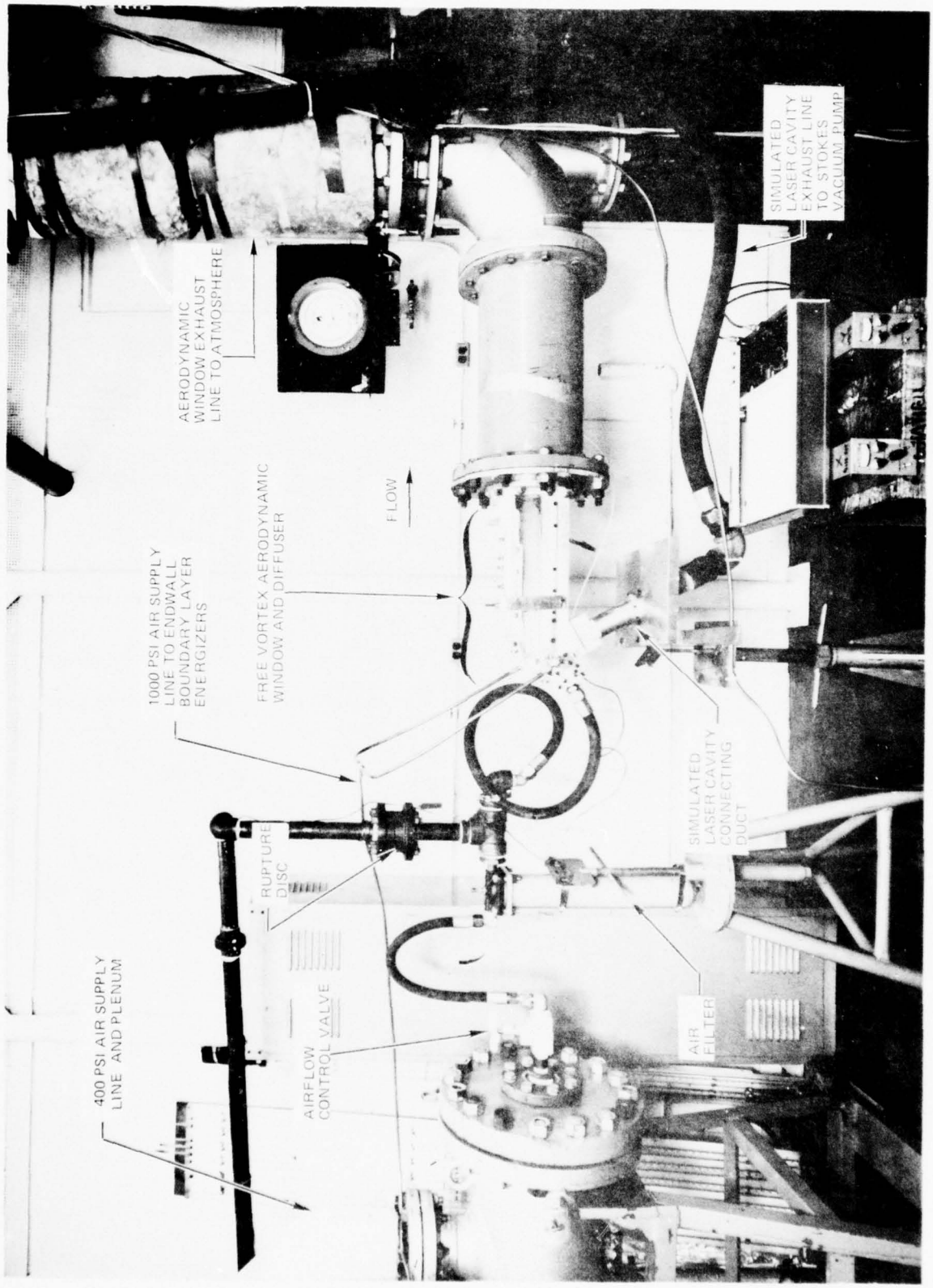

77-263-A

77-08-20-1

TYPICAL PRESSURE SUPPORT CHARACTERISTIC

3.49-cm DIA CIRCULAR APERTURE

$\dot{W}_L$=0 gm/sec

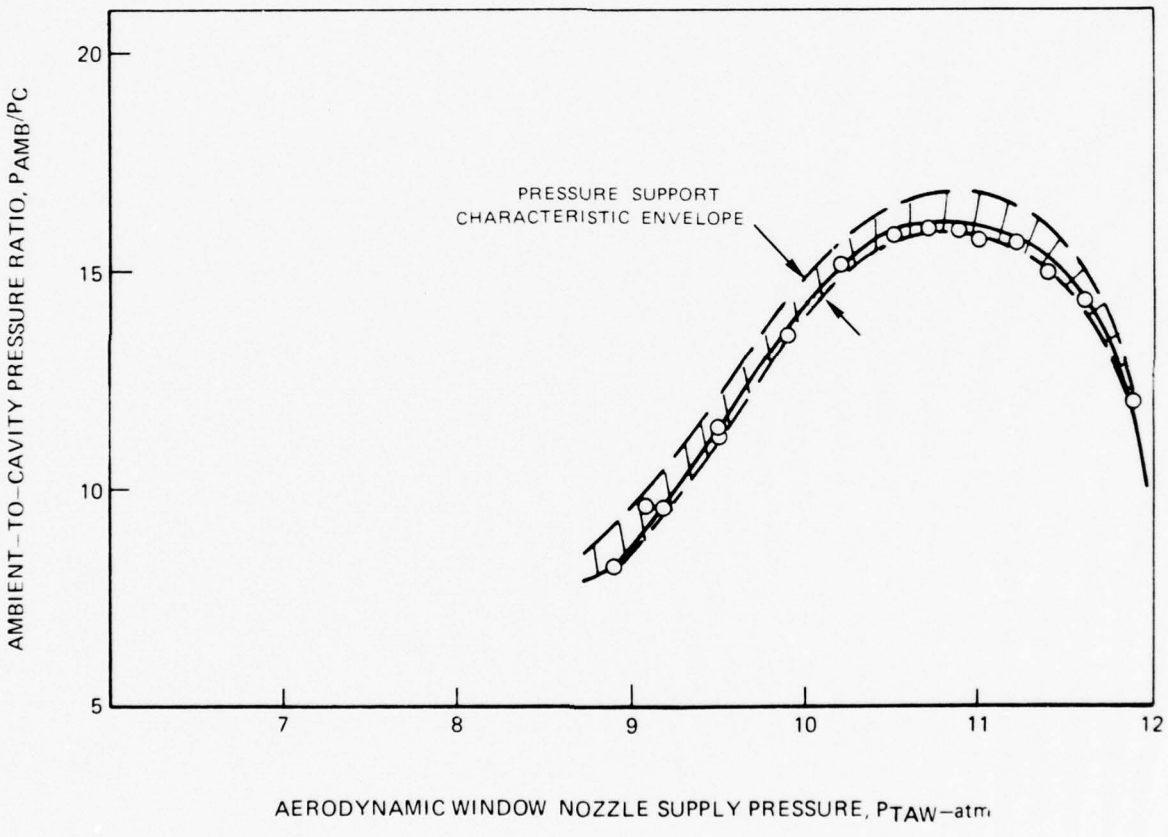

FIG. 7

FLOW VISUALIZATION TECHNIQUE

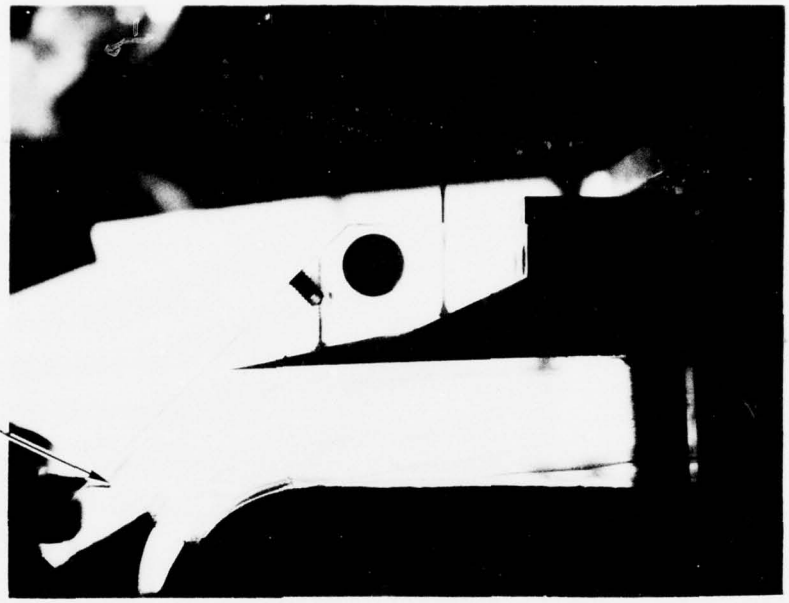

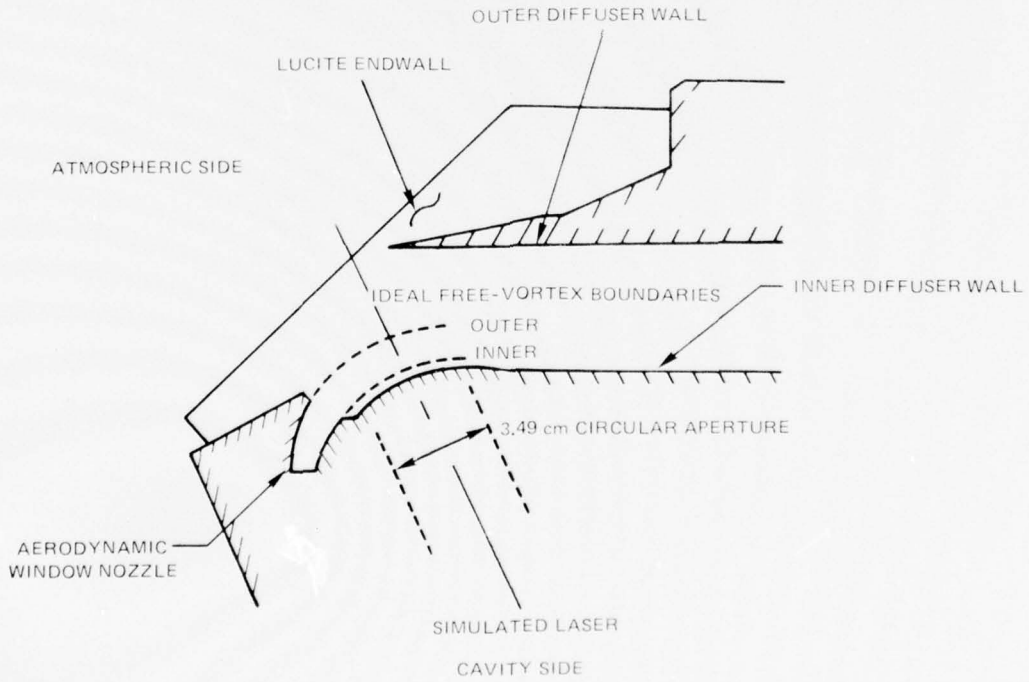

77-08-93-4

FIG. 8

PHOTOGRAPH OF ENDWALL FLOW PATTERN FOR 3.80 – cm SQUARE CROSS–SECTION APERTURE

P_{TAW} = 10 atm

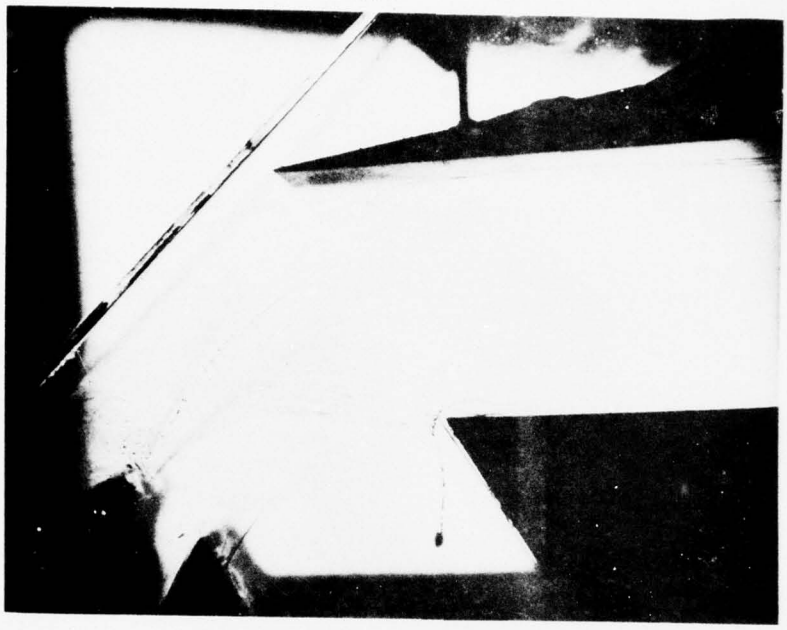

a. ZERO CAVITY LEAKAGE FLOW REMOVAL, $\dot{W}_L$ = 0 gm/sec

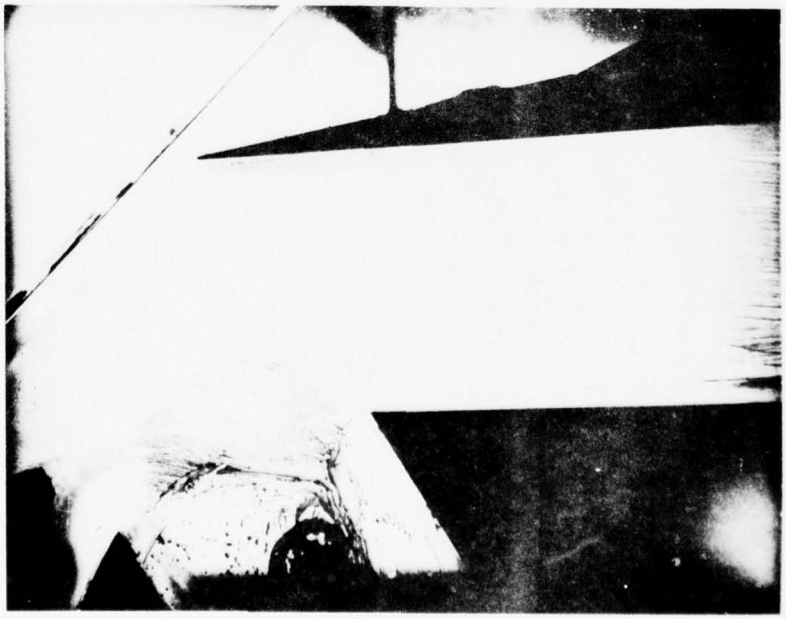

b. CAVITY LEAKAGE FLOW REMOVAL, $\dot{W}_L$ = 1.8 gm/sec

77–08–93–1

R77-912076-3

ENDWALL FLOW PATTERN FOR 3.80-cm SQUARE APERTURE WITH ZERO LEAKAGE REMOVAL

$\dot{W}_L$ = 0 gm/sec

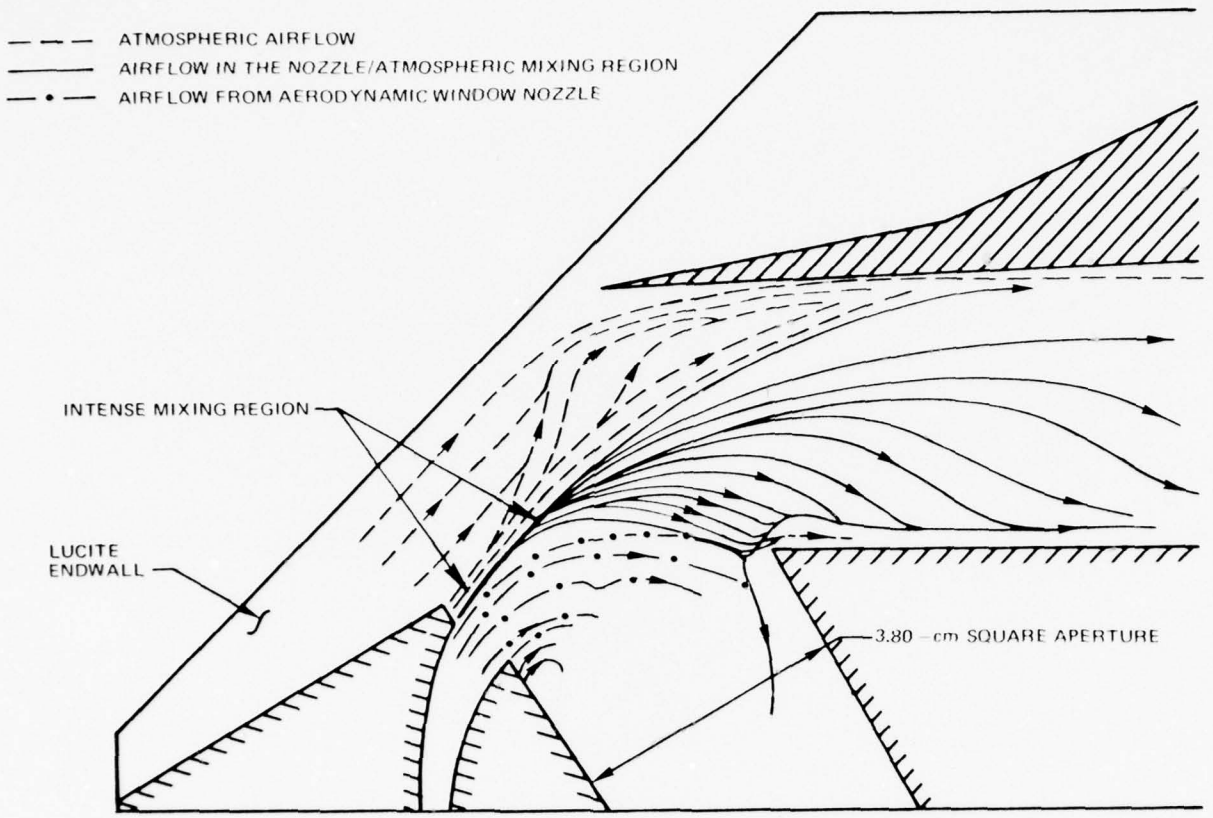

77-08-85-1

FIG. 9

ENDWALL FLOW PATTERN FOR 3.80 – cm SQUARE APERTURE WITH LEAKAGE REMOVAL

$\dot{W}_L$ = 1.9 gm/sec

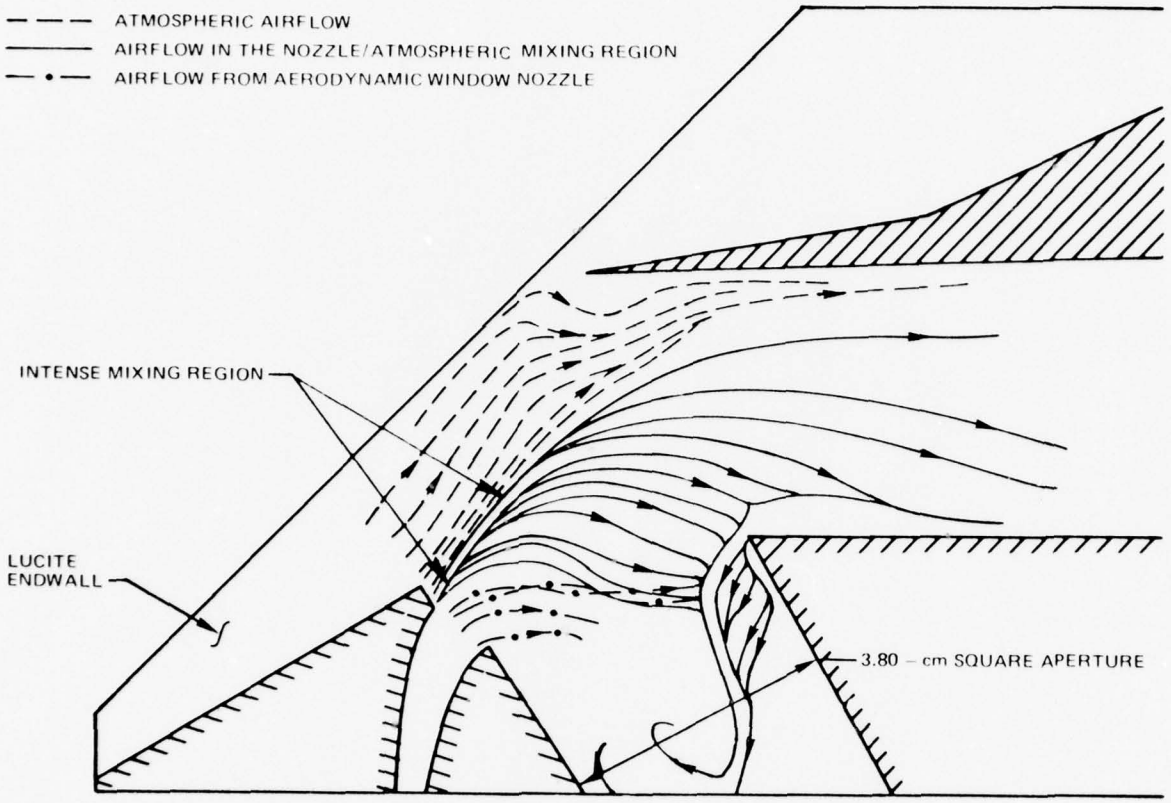

77-08-85-2

FIG. 10

FIG. 11

PHOTOGRAPH OF ENDWALL FLOW PATTERN FOR 3.49–cm DIA APERTURE

P_{TAW} = 10 atm

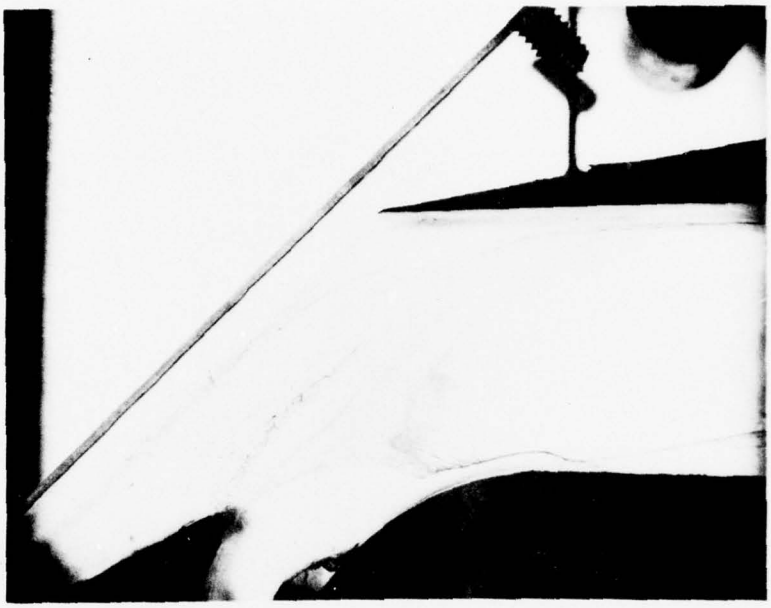

a. ZERO CAVITY LEAKAGE FLOW REMOVAL, $\dot{W}_L$ = 0 gm/sec

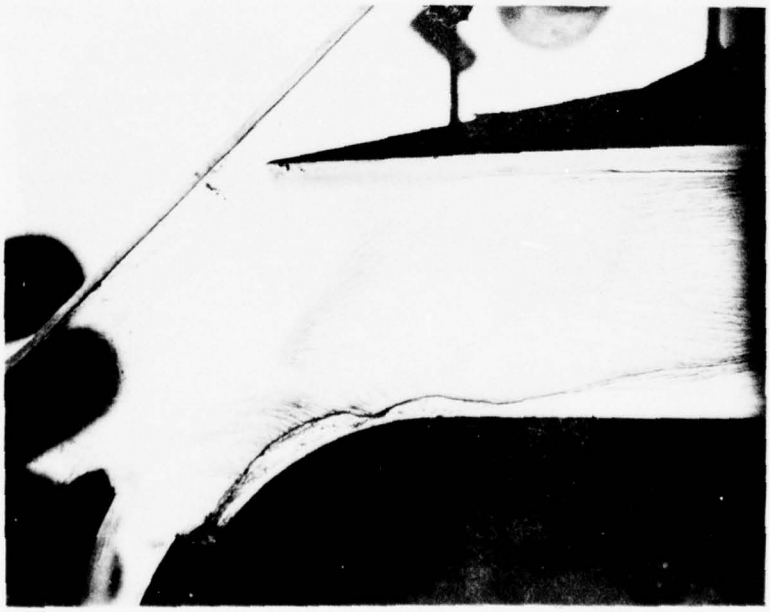

b. CAVITY LEAKAGE FLOW REMOVAL, $\dot{W}_L$ = 1.6 gm/sec

77–08–93–2

ENDWALL FLOW PATTERN FOR 3.49 – cm DIA CIRCULAR APERTURE WITH ZERO LEAKAGE REMOVAL

$\dot{W}_L = 0$ gm/sec

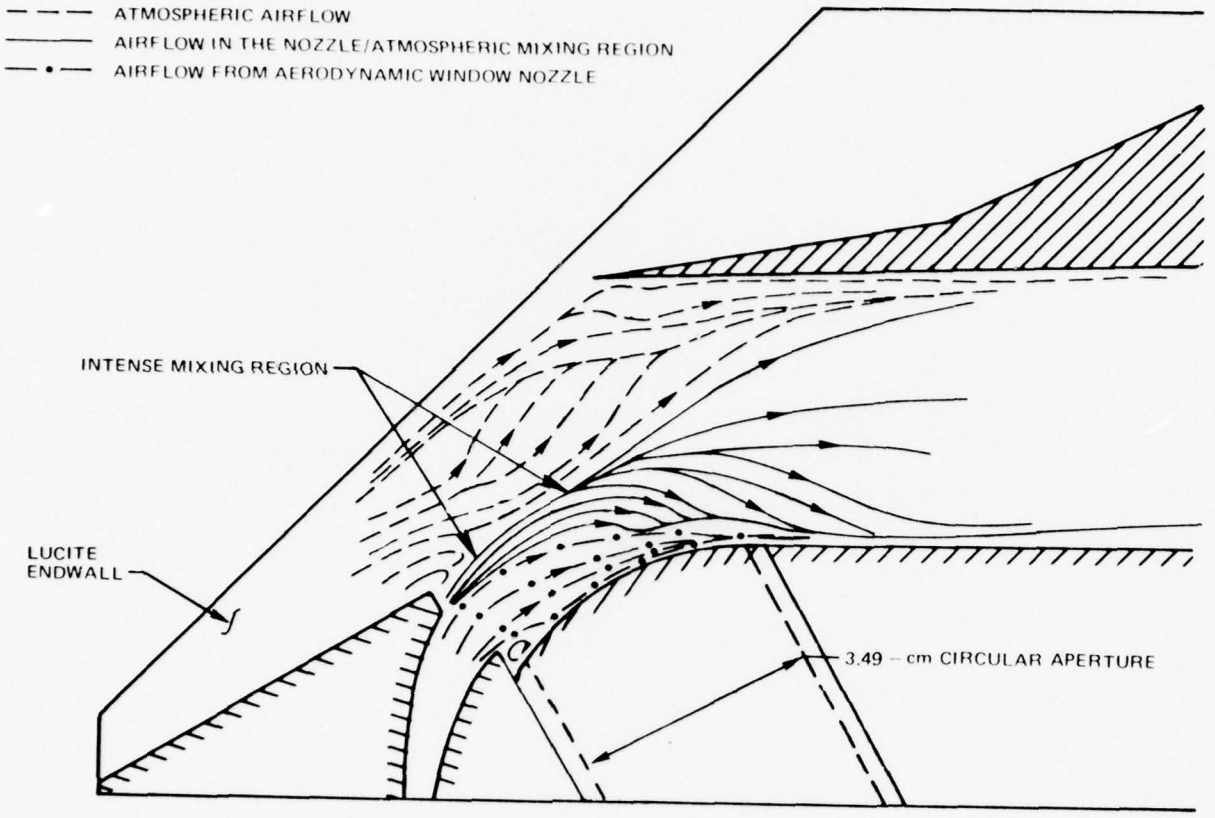

FIG. 12

R77-912076-3

ENDWALL FLOW PATTERN FOR 3.49 – cm DIA CIRCULAR APERTURE WITH LEAKAGE REMOVAL

$\dot{W}_L$ = 1.8 gm/sec

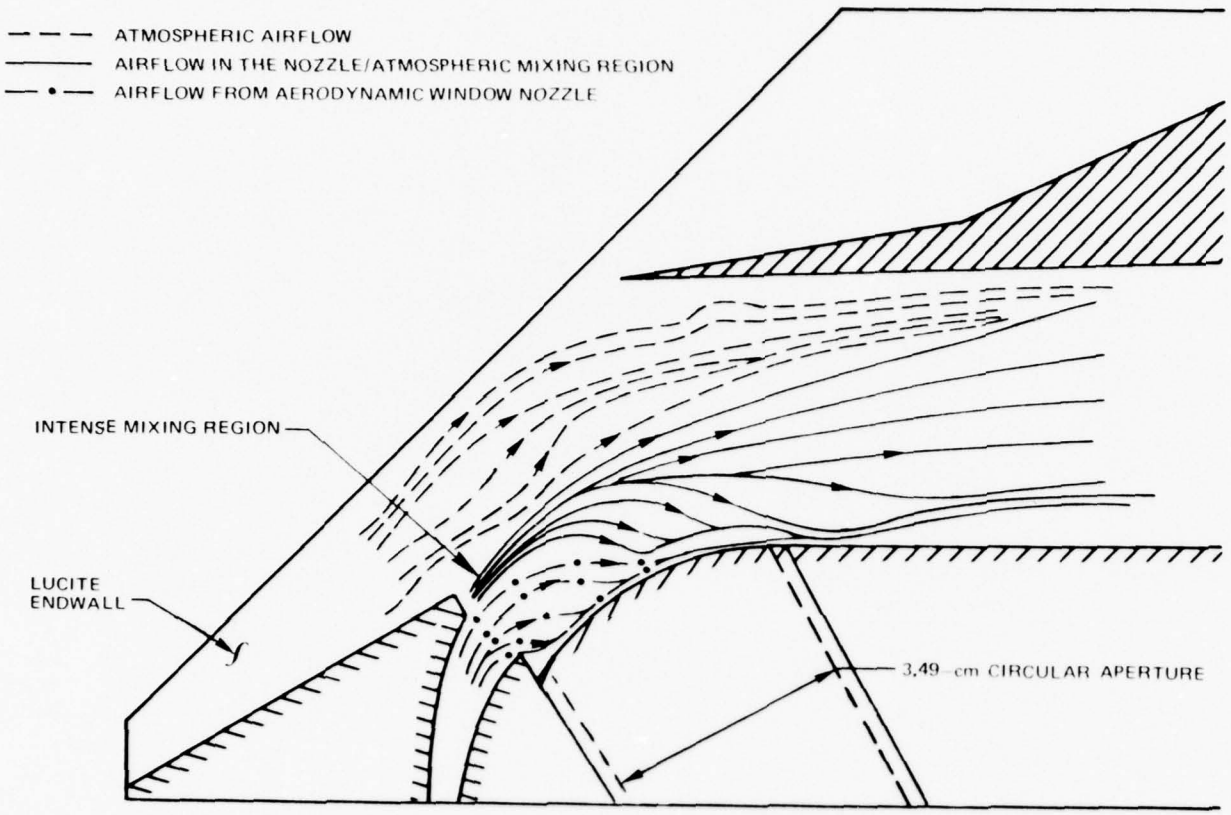

77-08-85-4

FIG. 13

PRESSURE SUPPORT CHARACTERISTIC OF FREE-VORTEX AERODYNAMIC WINDOW WITH VARIOUS APERTURE CONFIGURATIONS

$\dot{W}_L$ = 0 gm/sec

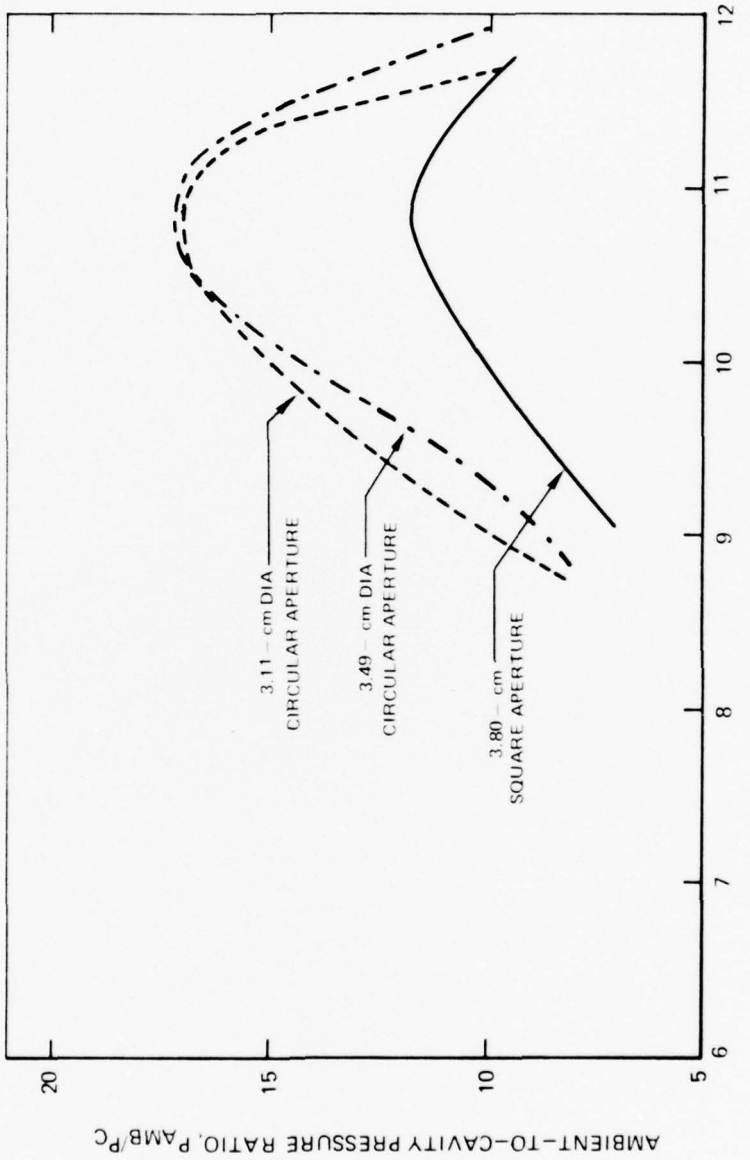

77-08-93-3

FIG. 15

PITOT PRESSURE PROBE AND TRAVERSING ASSEMBLY

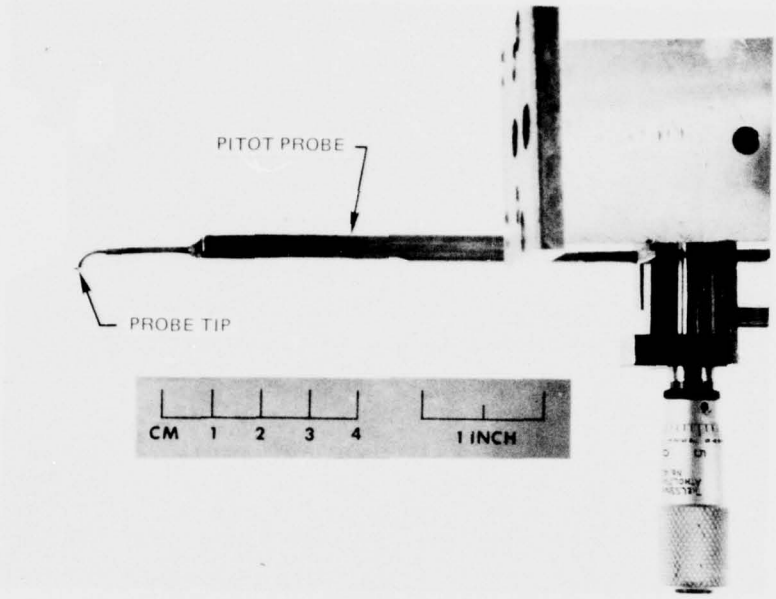

a) PITOT PRESSURE PROBE

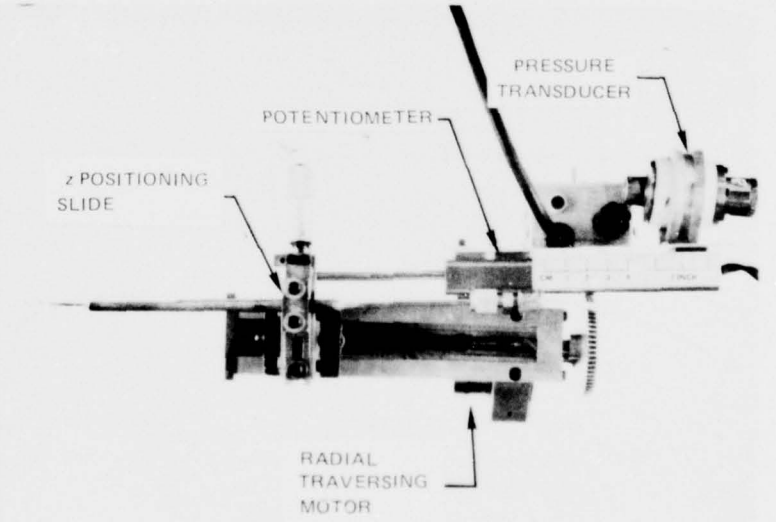

b) PROBE TRAVERSING ASSEMBLE

77–08–80–3

FIG. 16

TYPICAL PITOT PRESSURE DISTRIBUTIONS

VARIOUS DISTANCES FROM THE ENDWALL, z

3.49-cm DIA CIRCULAR APERTURE

$\Delta\theta$ = 0 DEG (NOZZLE EXIT PLANE)

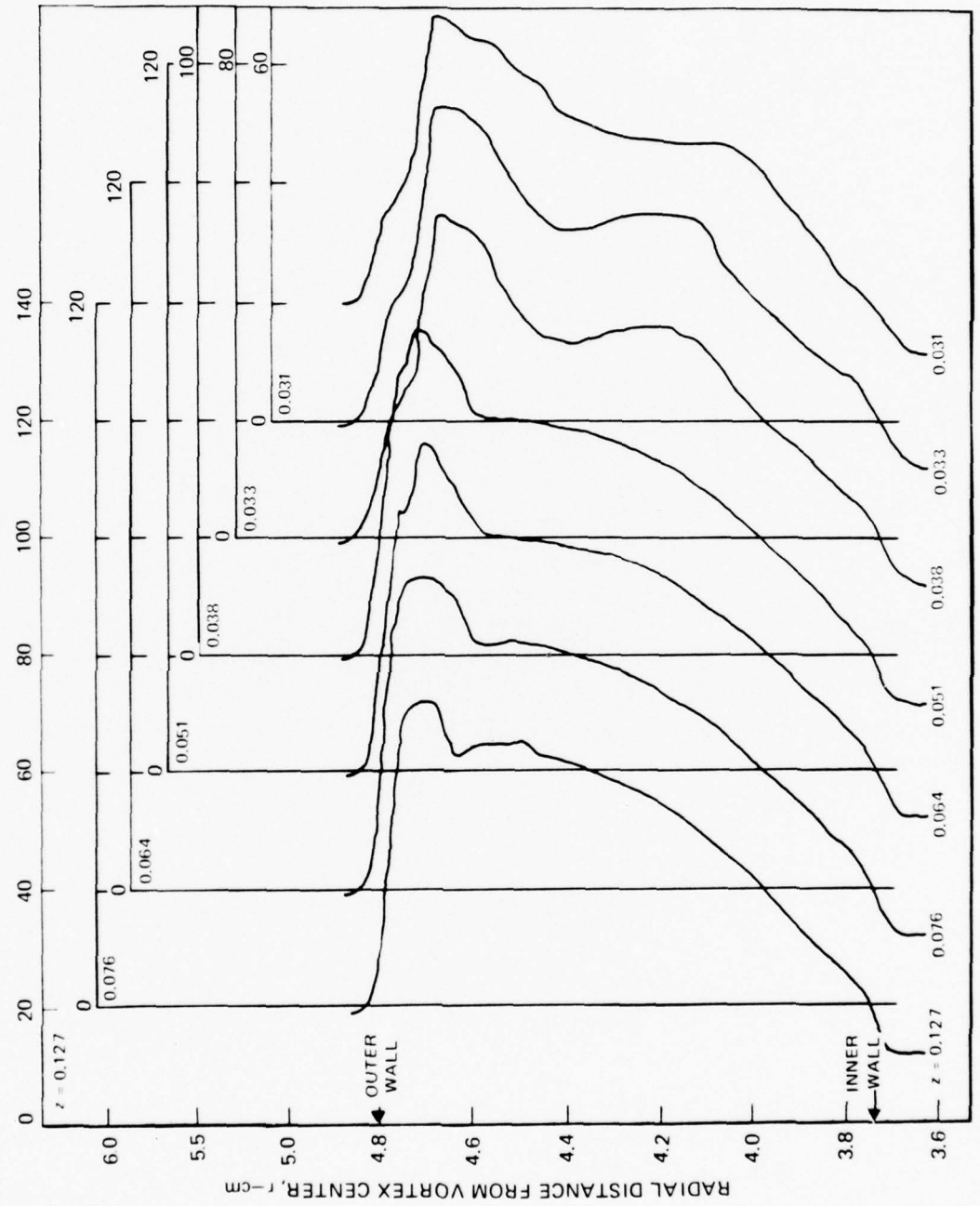

77-07-250-5

FREE STREAM PITOT PRESSURE AT NOZZLE EXIT PLANE

WITH NO CAVITY LEAKAGE REMOVAL

3.49 – cm DIA. CIRCULAR APERTURE

$\dot{W}_L$ = 0 gm/sec
$\Delta\theta$ = 0 DEG
z = 1.194 cm

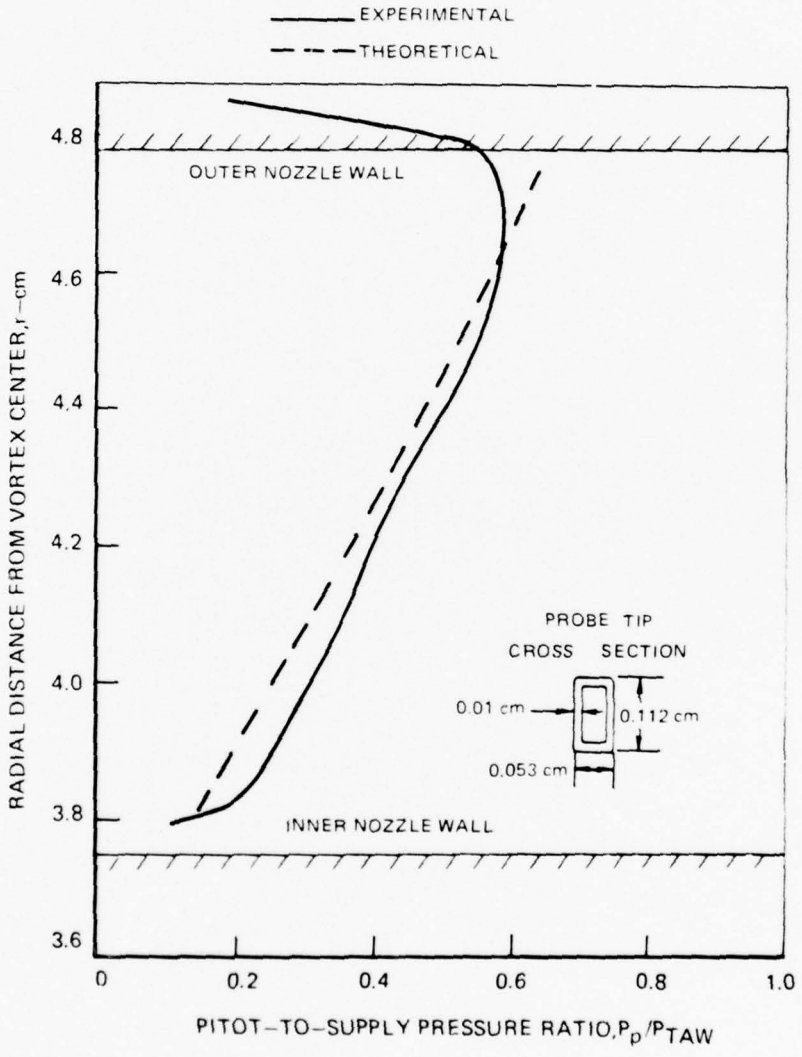

77-08-6-2

FREE STREAM PITOT PRESSURE ALONG LASER BEAM AXIS

WITH NO CAVITY LEAKAGE REMOVAL

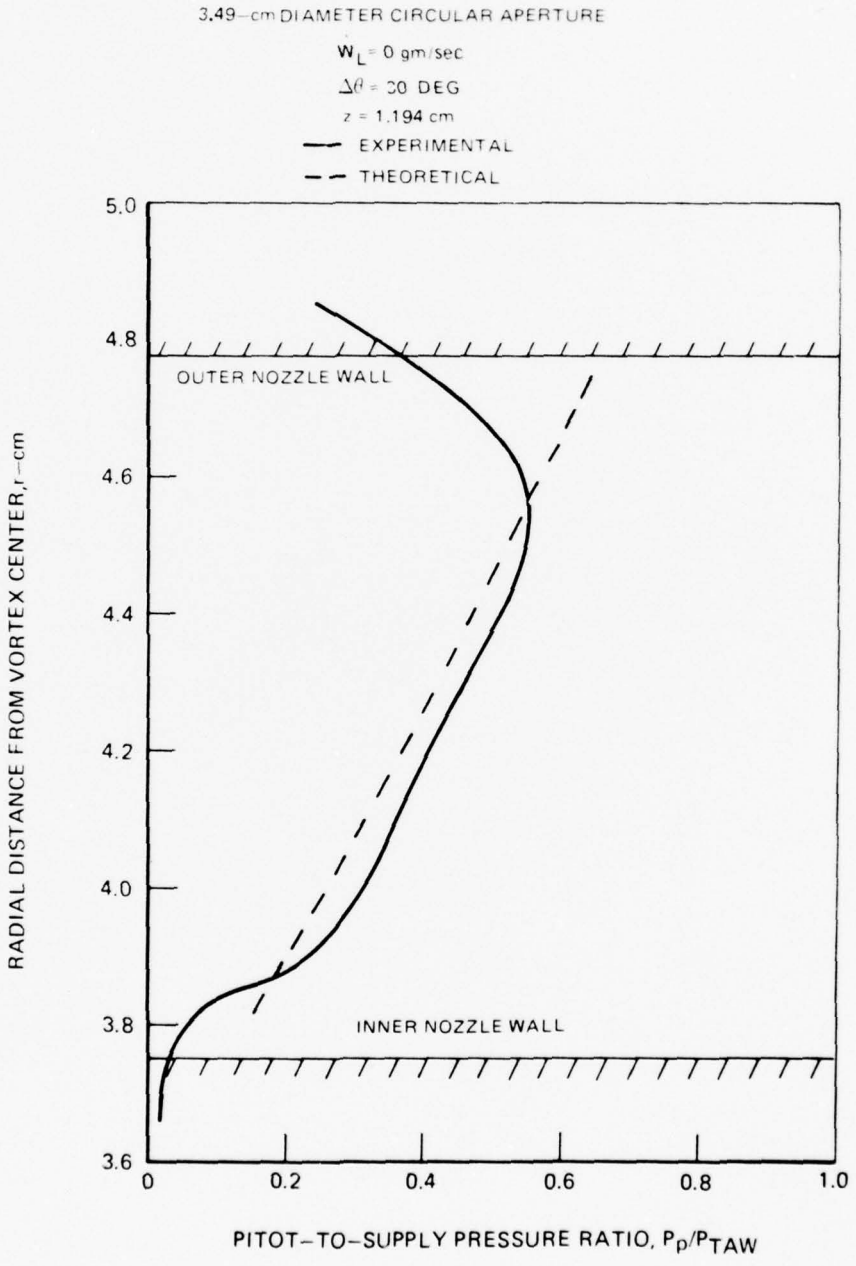

77-08-6-3

FIG. 19

FREE STREAM PITOT PRESSURE AT $\Delta\theta$ = 60 DEG WITH NO CAVITY LEAKAGE REMOVAL

3.4 9-cm DIA CIRCULAR APERTURE

$\dot{W}_L$ = 0 gm/sec

$\Delta\theta$ = 60 DEG

z = 1.194 cm

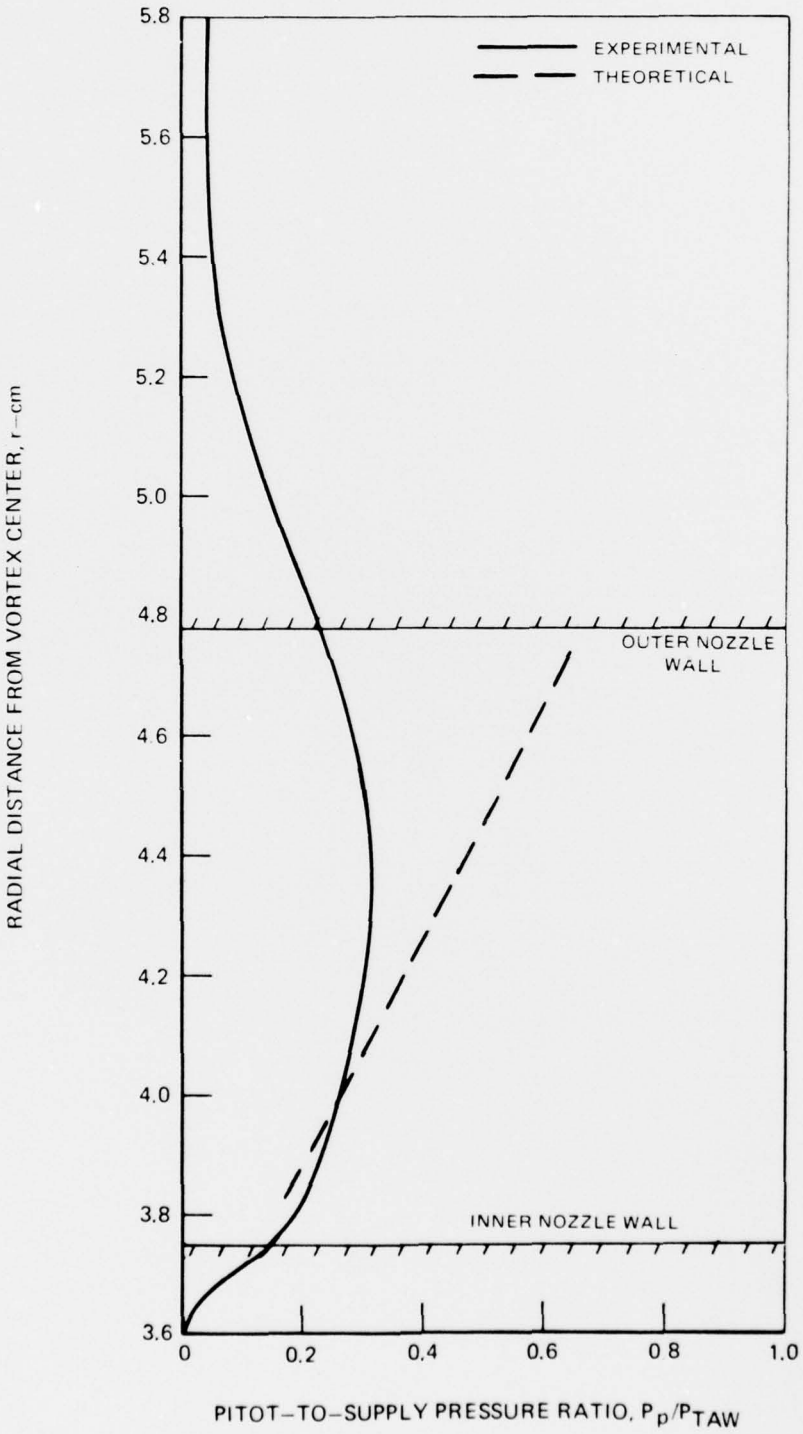

77-08-80-1

FREE STREAM PITOT PRESSURE ALONG LASER BEAM AXIS

WITH CAVITY LEAKAGE REMOVAL

3.49-cm DIA CIRCULAR APERTURE

$\dot{W}_L$ = 1.6 gm/sec

$\Delta\theta$ = 30 DEG

z = 1.194 cm

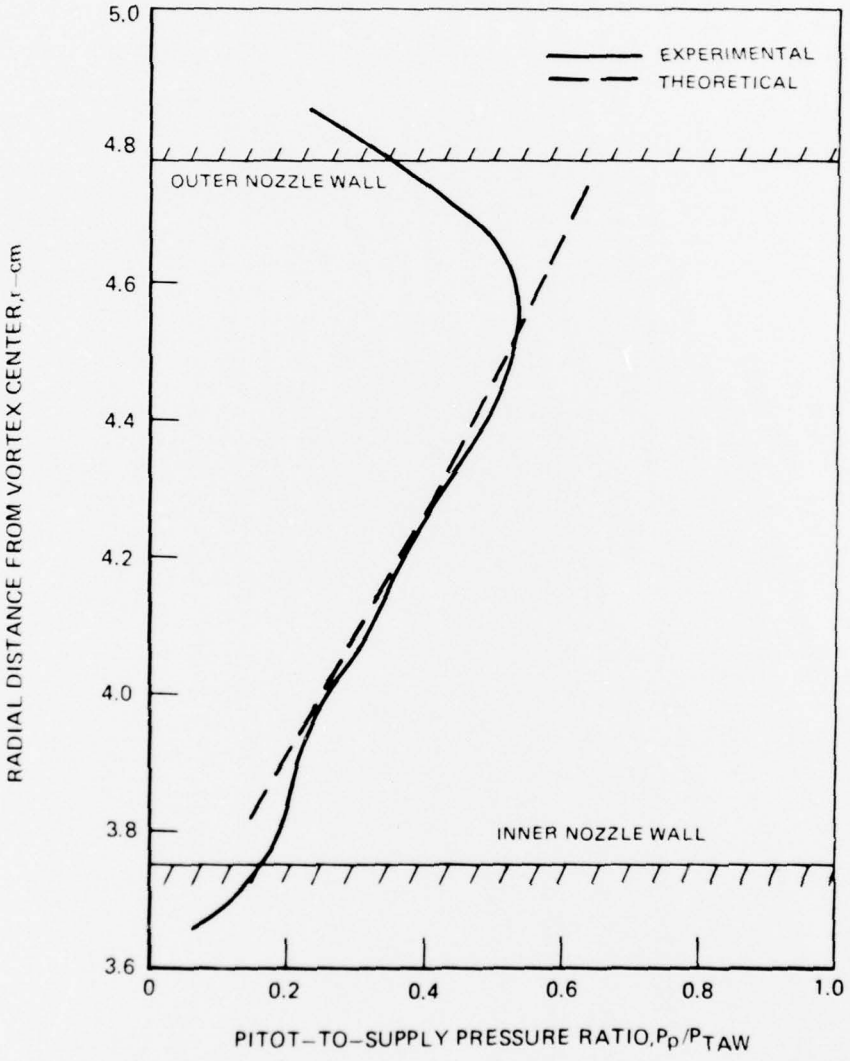

77-08-6-1

FREE STREAM PITOT PRESSURE AT $\Delta\theta$ = 60 WITH CAVITY LEAKAGE REMOVAL

3.49- cm DIA CIRCULAR APERTURE
$\dot{W}_L$ = 1.6 gm/sec
$\Delta\theta$ = 60 DEG
z = 1.194 cm

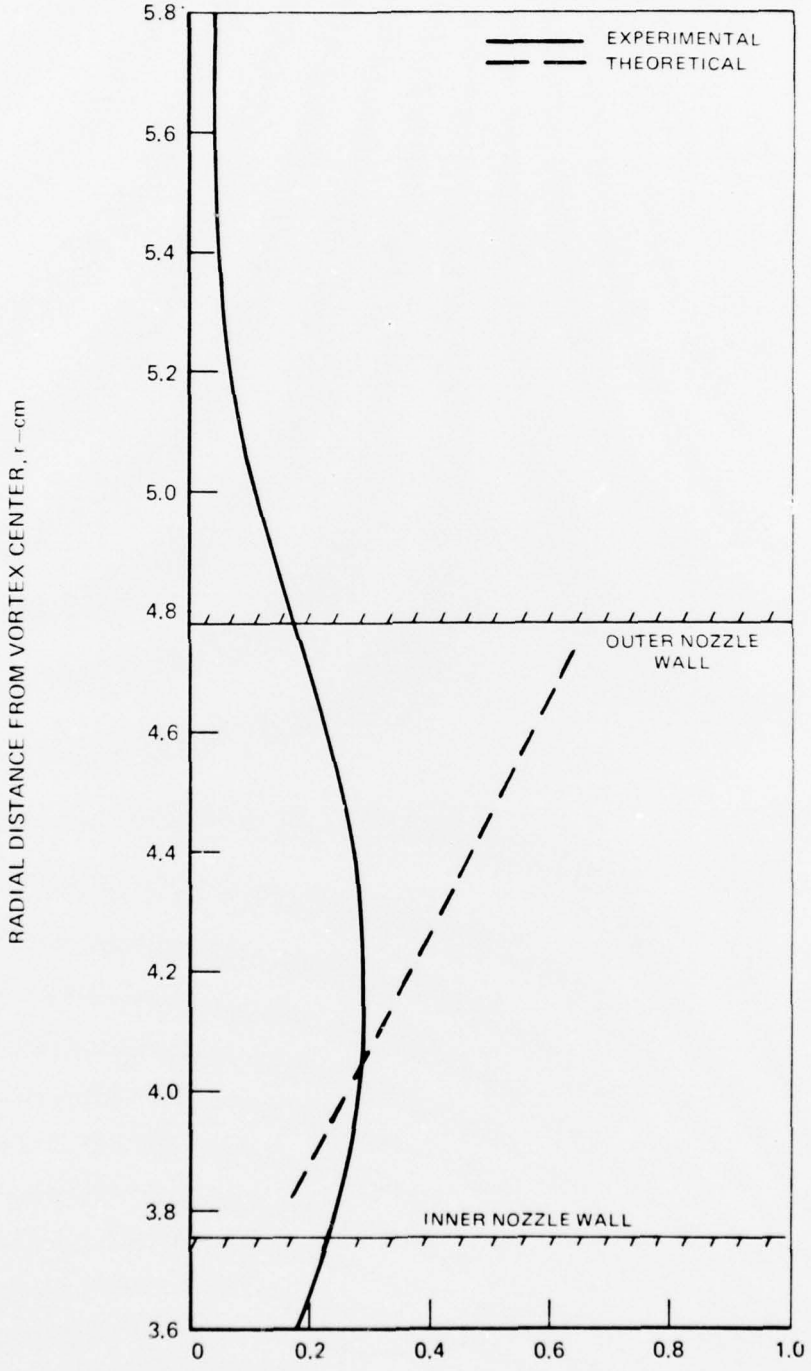

77-08-80-2

ENDWALL PITOT PRESSURE DISTRIBUTION FOR 3.80-cm SQUARE APERTURE

$\Delta\theta$=0 DEG

○ $\dot{W}_L$=0

□ $\dot{W}_L$=1.6 gm/sec

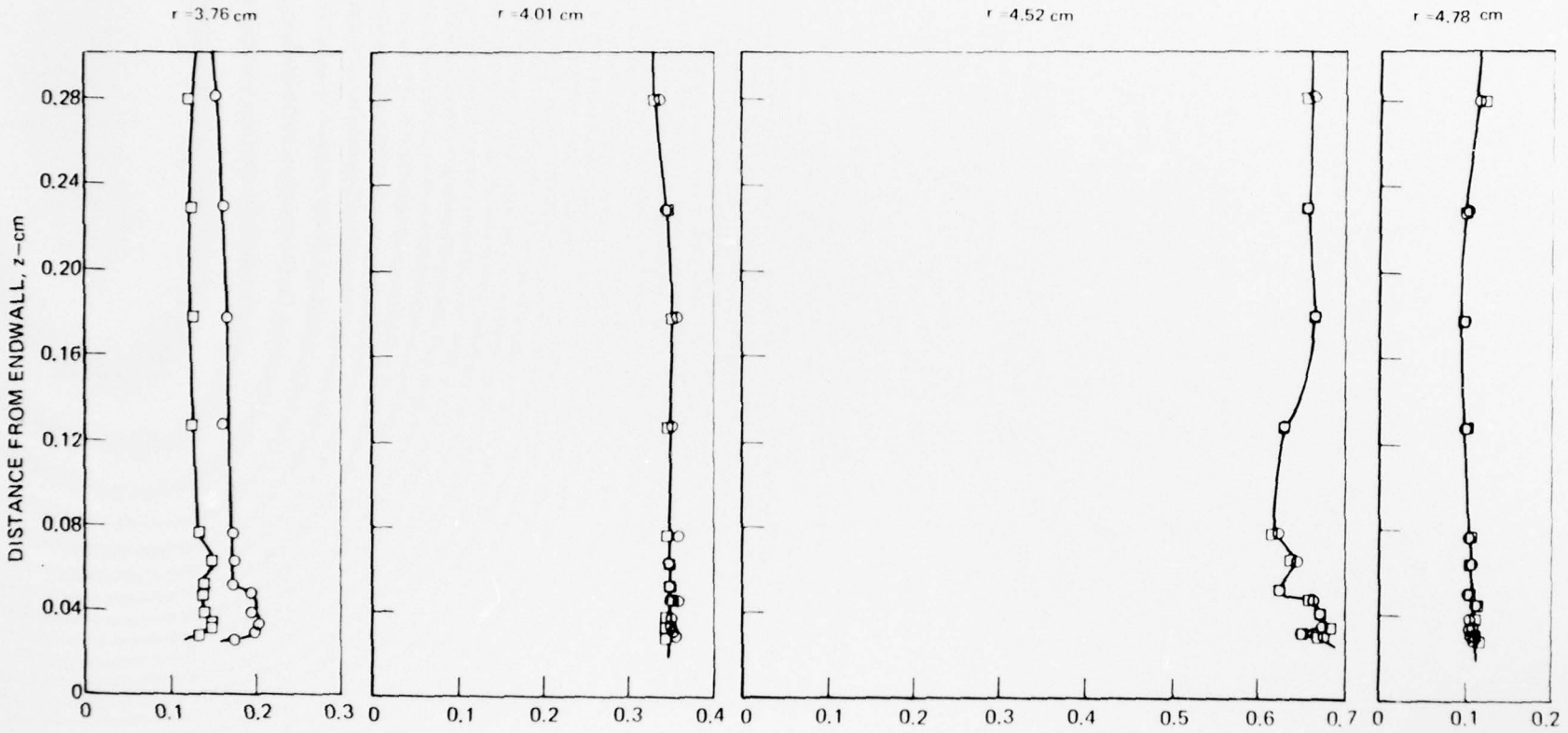

77-08-36-4

FIG. 22a

ENDWALL PITOT PRESSURE DISTRIBUTION FOR 3.80–cm SQUARE APERTURE

$\Delta\theta$=30 DEG

○ $\dot{W}_L$=0

□ $\dot{W}_L$=1.6 gm/sec

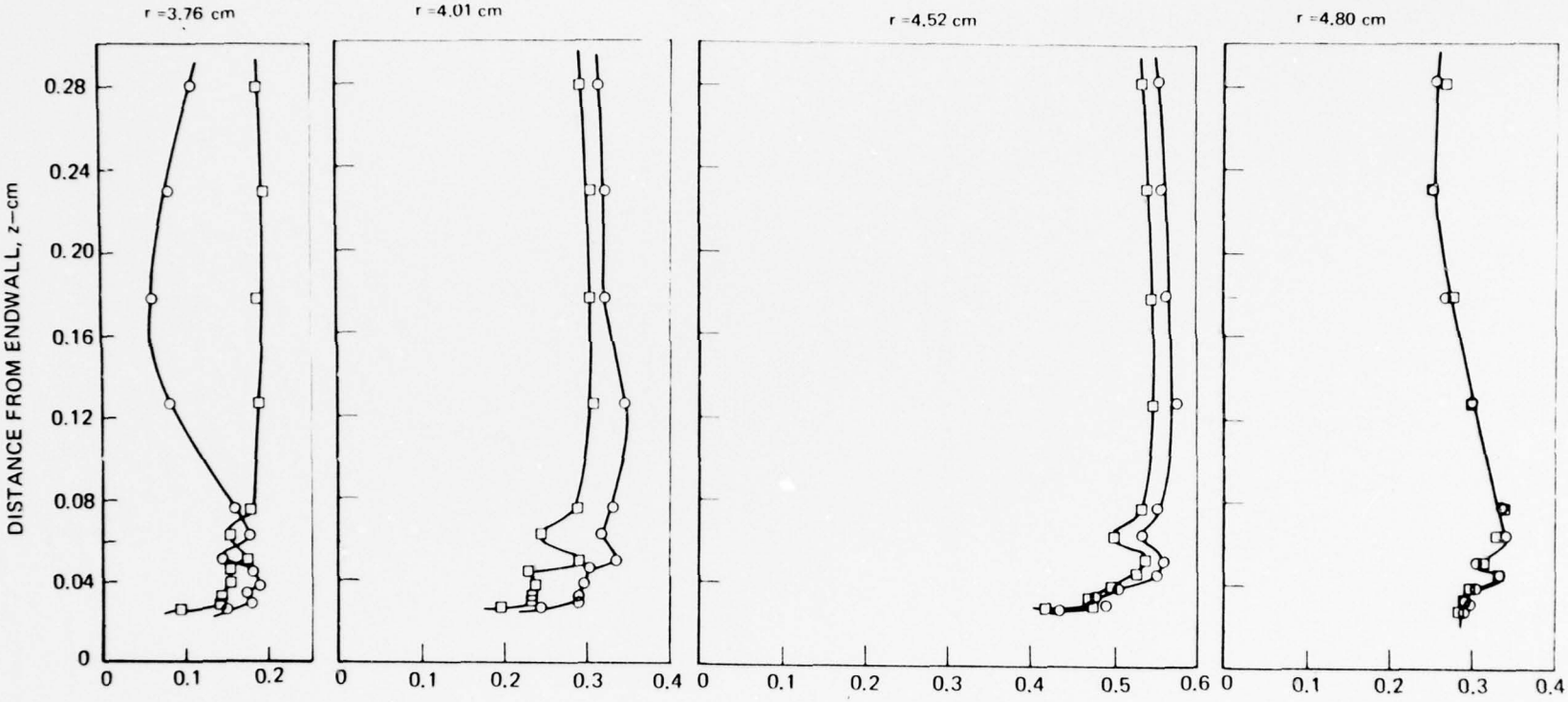

PITOT–TO–SUPPLY PRESSURE RATIO, P_p/P_{TAW}

77-08-36-6

FIG. 22b

ENDWALL PITOT PRESSURE DISTRIBUTION FOR 3.80-cm SQUARE APERTURE

$\Delta\theta$=60 DEG

○ $\dot{W}_L$=0

□ $\dot{W}_L$=1.6 gm/sec

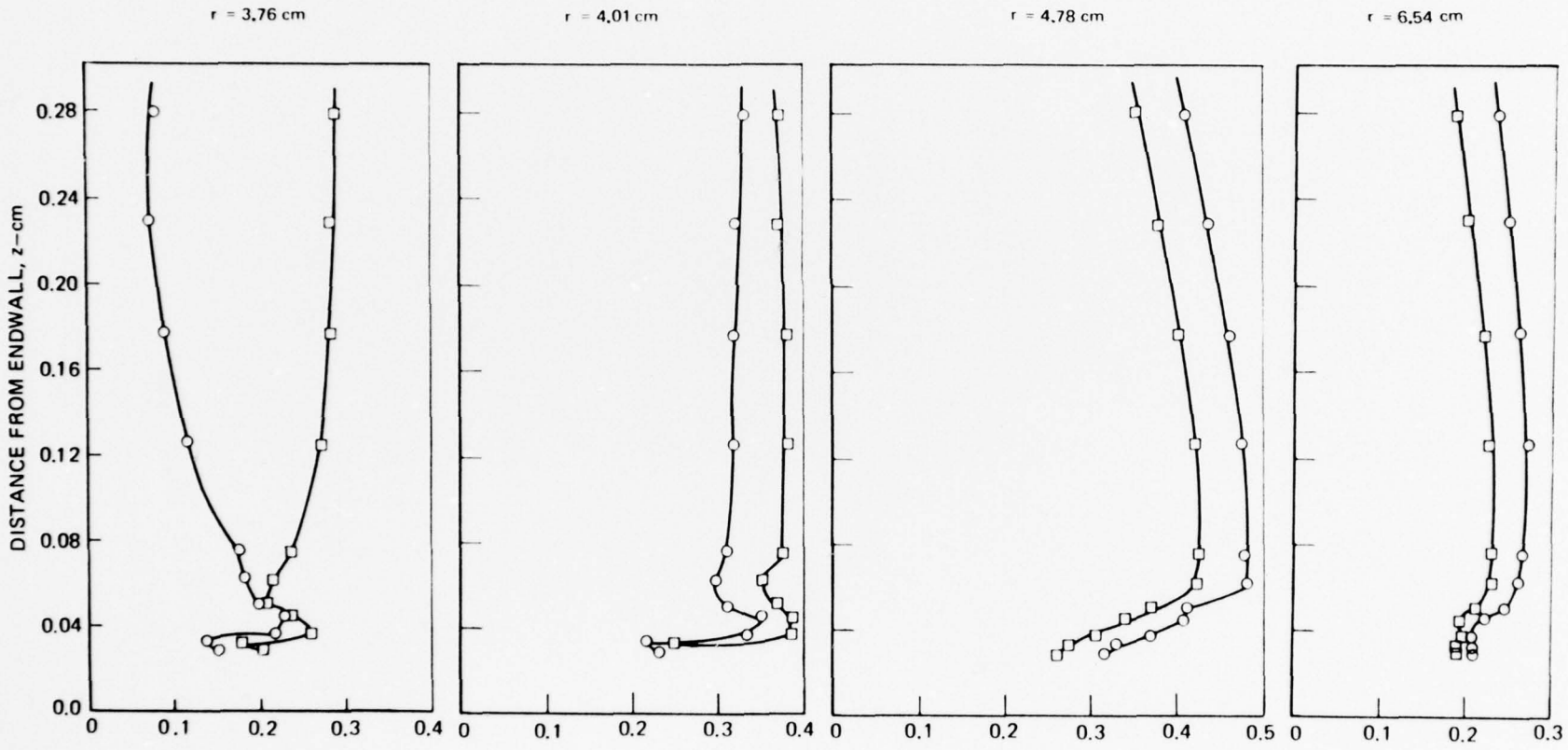

77-08-36-5

FIG. 22c

FIG. 23 a

ENDWALL PITOT PRESSURE DISTRIBUTION FOR 3.49–cm DIA CIRCULAR APERTURE

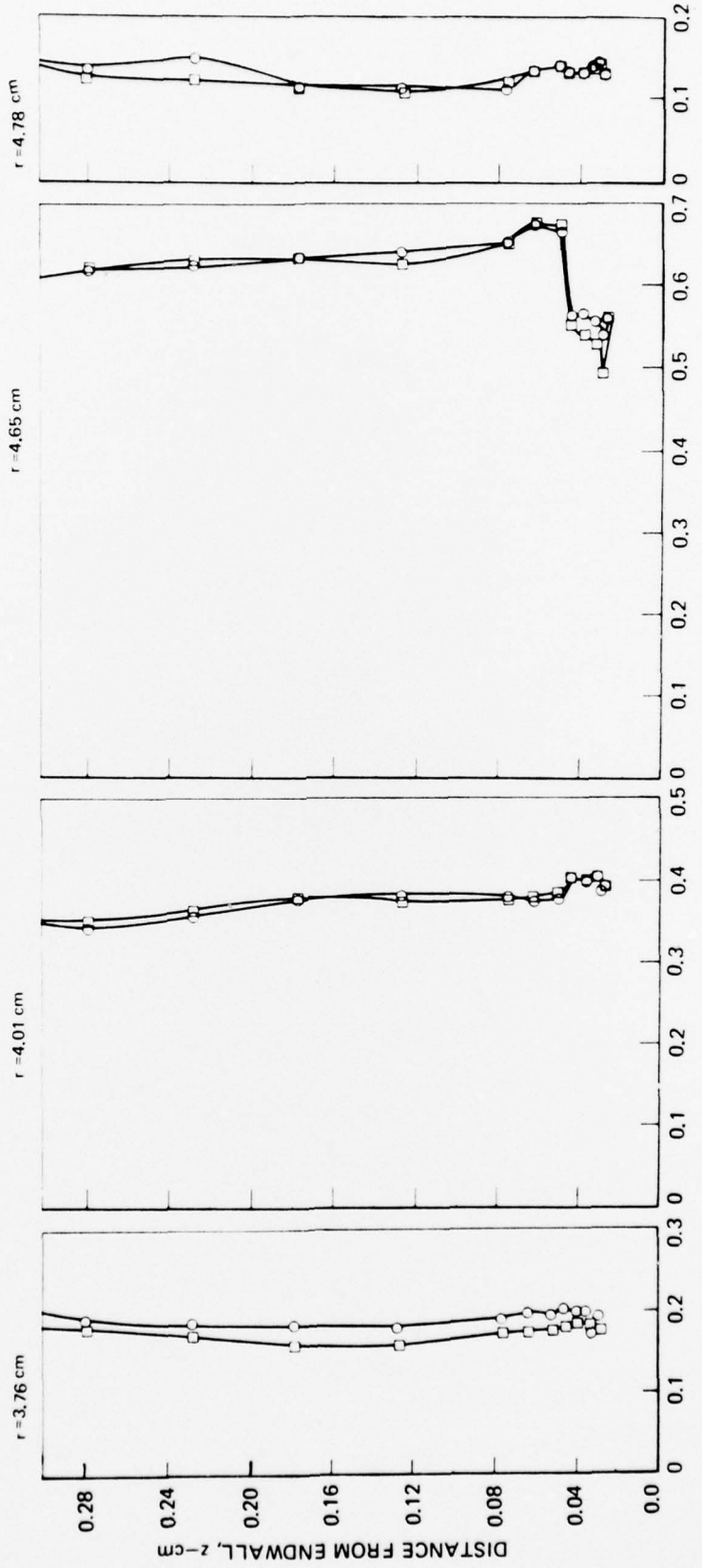

77–08–36–3

FIG. 23b

PITOT PRESSURE PROFILE NORMAL TO ENDWALL FOR 3.49-cm DIA. CIRCULAR APERTURE

$\Delta\theta$ = 30 DEG

$\dot{W}_L$ = 0 gm/sec

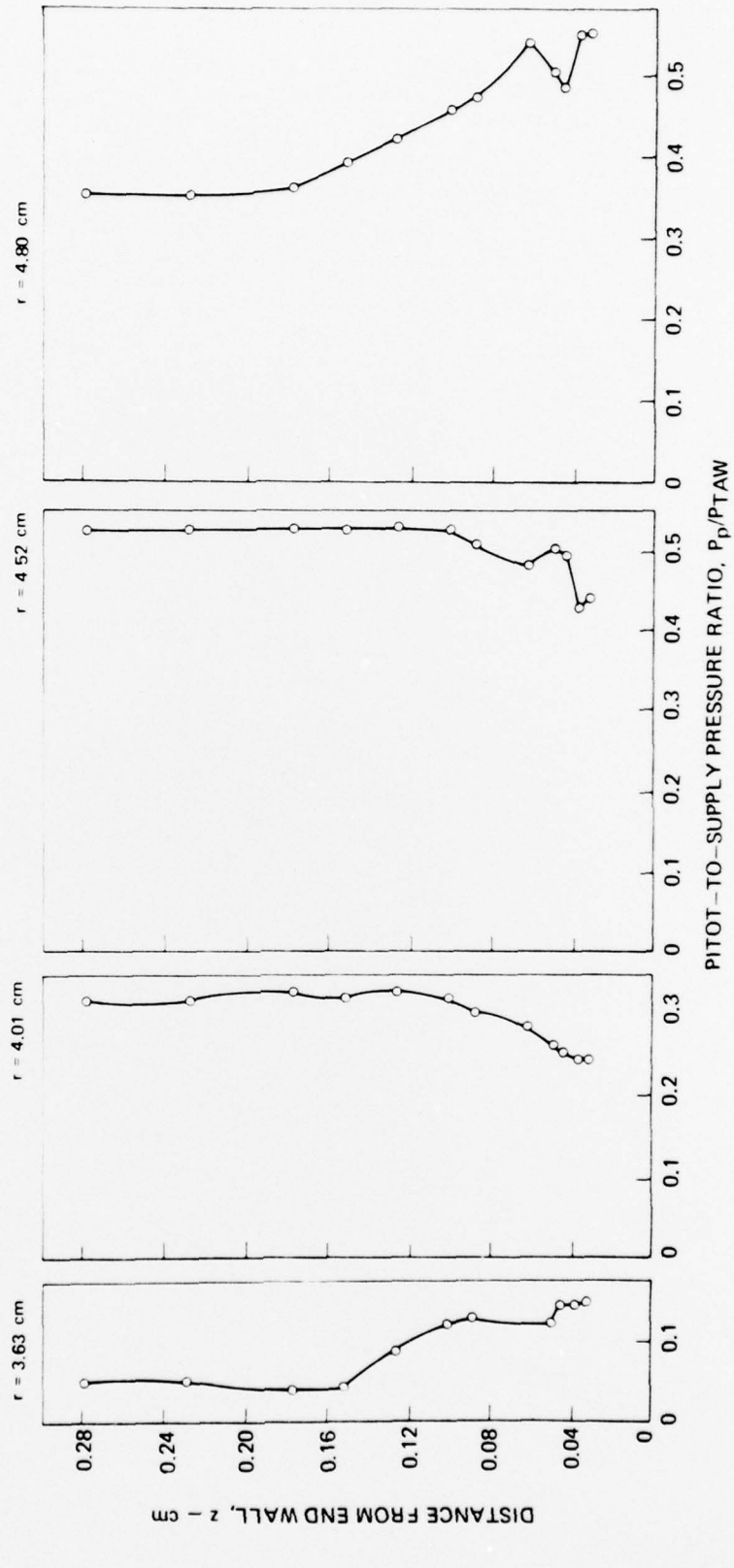

77-08-54-1

R77-912-076-3

PITOT PRESSURE PROFILE NORMAL TO ENDWALL FOR 3.49–cm DIA. CIRCULAR APERTURE

$\Delta\theta$ = 60 DEG

○ $\dot{w}_L$ = 0

□ $\dot{w}_L$ = 1.6 gm / sec

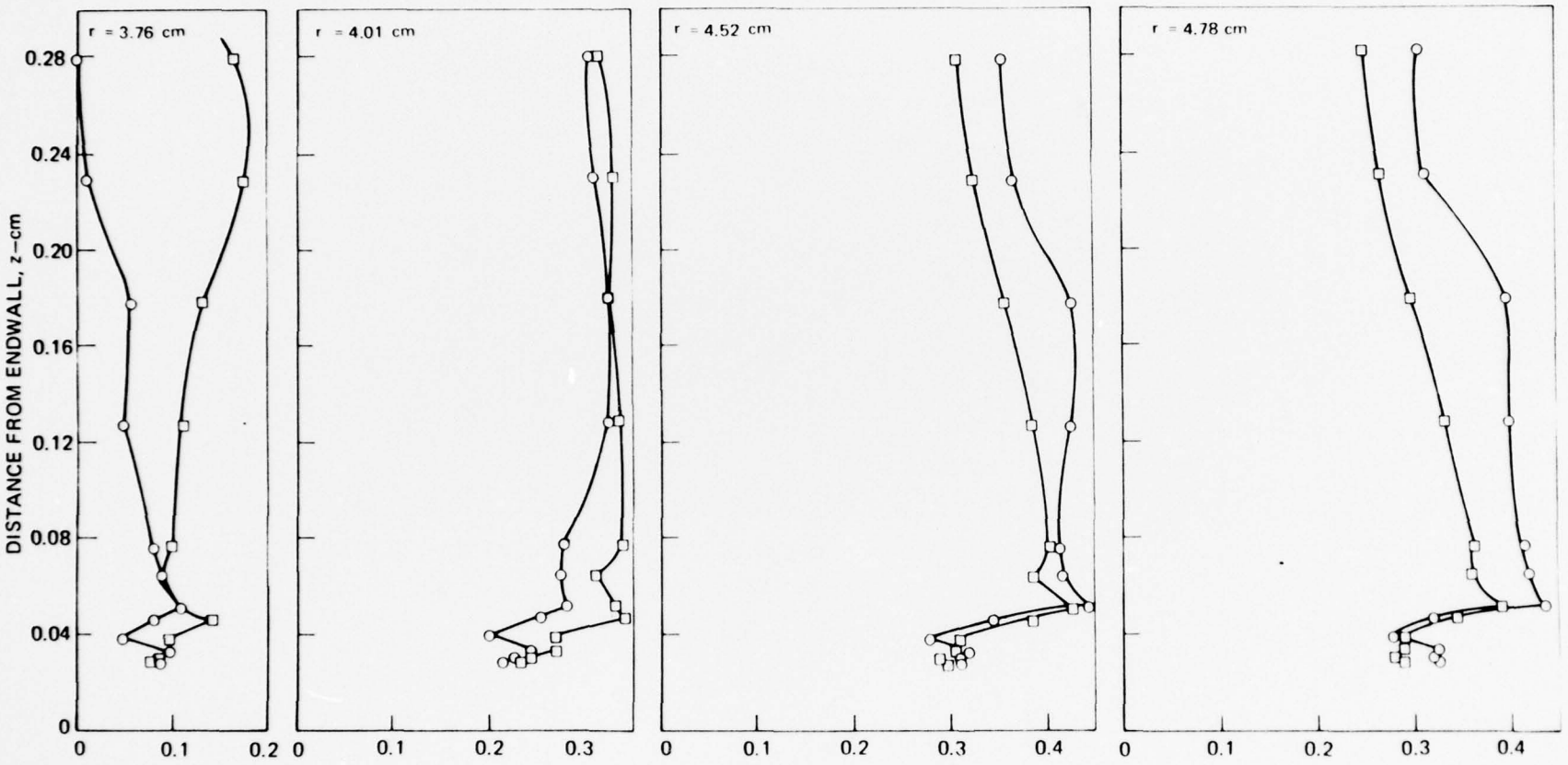

77-08-36-1

FIG. 23c

FIG. 24

ENDWALL BOUNDARY LAYER FLOW ENERGIZER

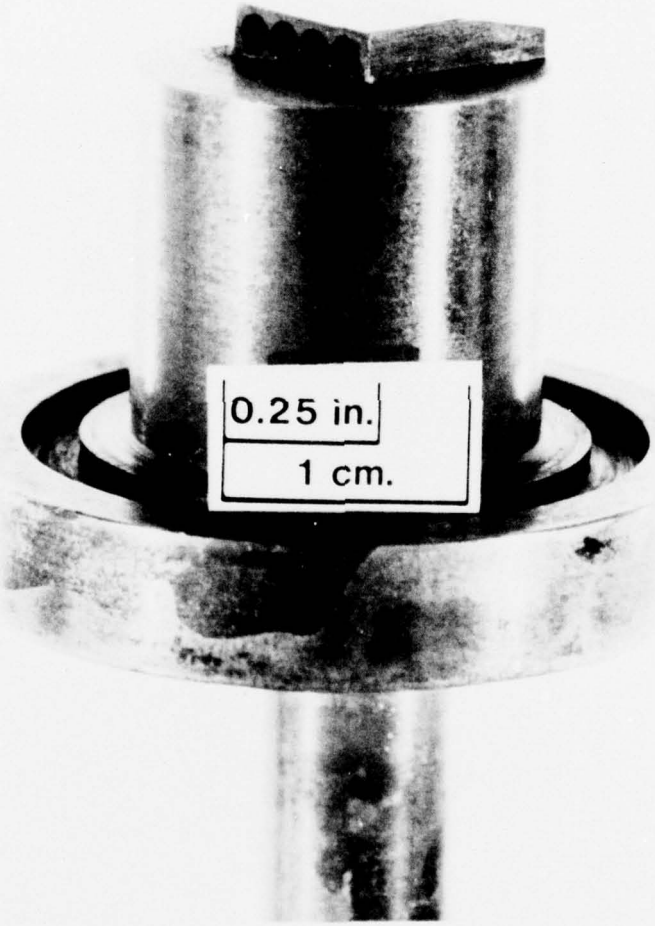

FIG. 25

ENDWALL BOUNDARY LAYER FLOW ENERGIZER INSTALLATION

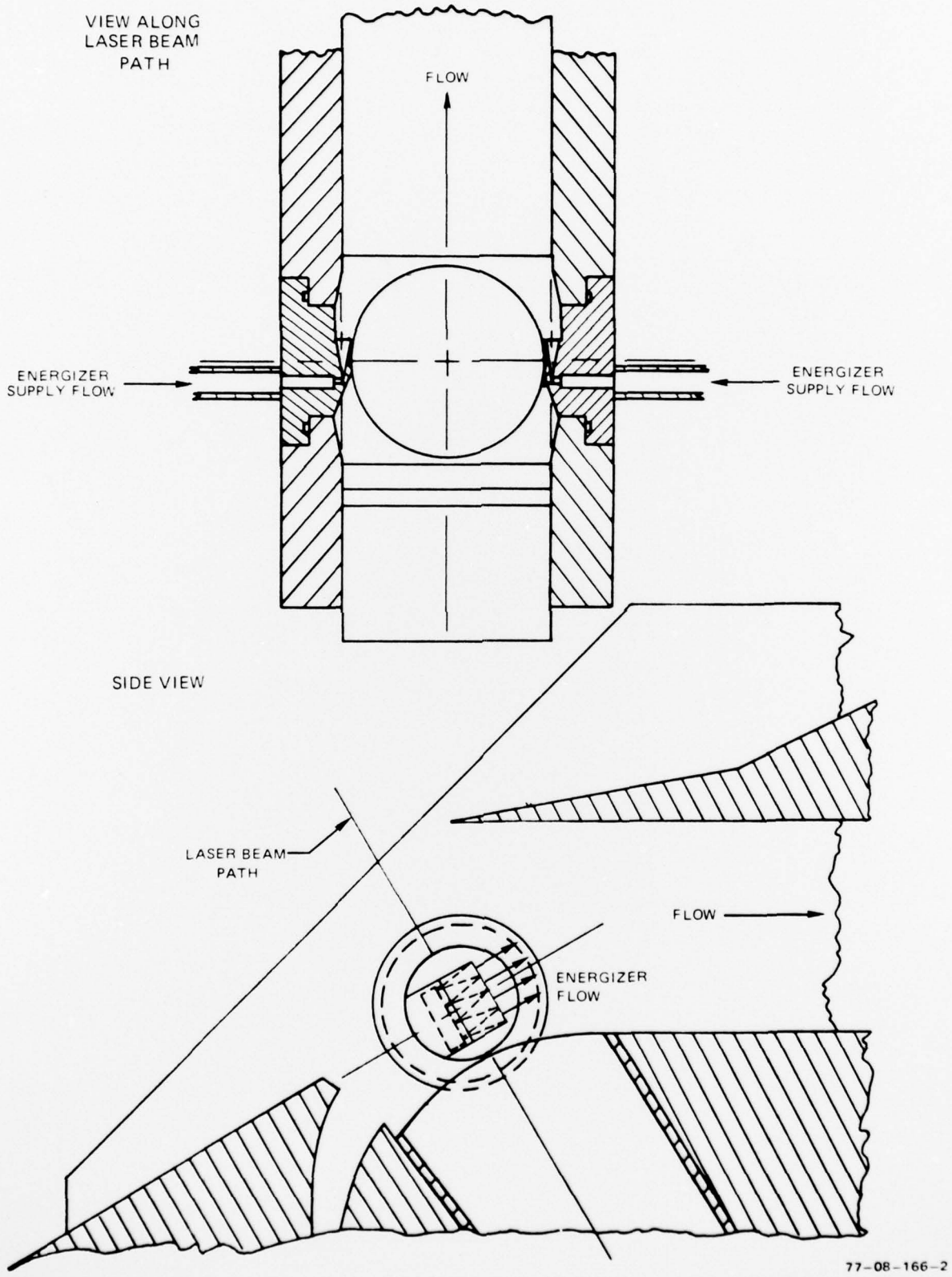

PRESSURE SUPPORT CHARACTERISTIC WITH END WALL FLOW ENERGIZERS INSTALLED

3.49–cm DIA APERTURE

ϕ = 90 DEG

$\dot{W}_L$ = 0 gm/sec

$\dot{W}_{ENG}$ = 0 gm/sec

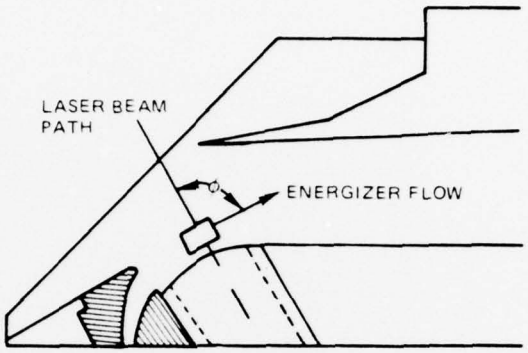

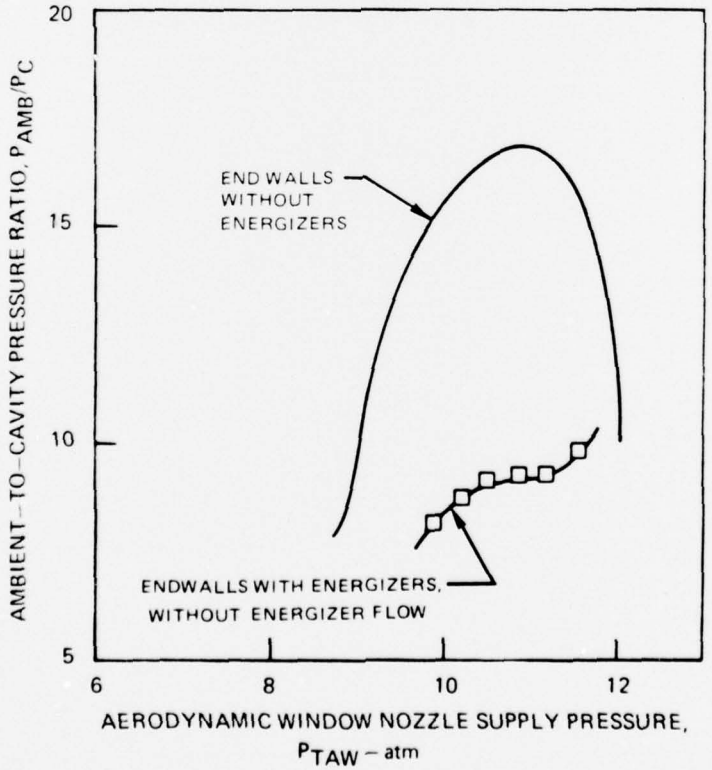

77–08–166–1

EFFECT OF ENDWALL ENERGIZER FLOW RATE ON LASER CAVITY LEAKAGE

3.49 – cm DIA CIRCULAR APERTURE

ϕ = 90 DEG

P_{TAW} = 11.5 atm

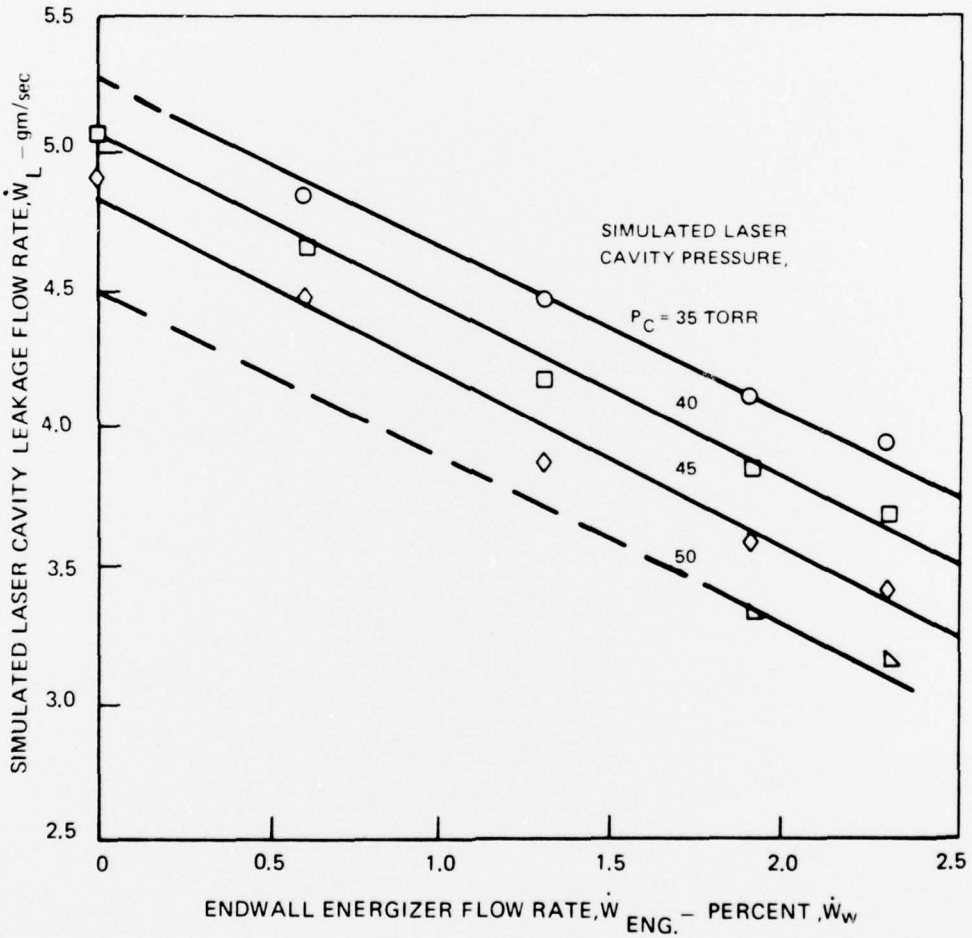

77–08–66–1

FIG. 28

EFFECT OF PURGE FLOW ON CAVITY PRESSURE

3.49 – cm DIA CIRCULAR APERTURE

OPEN SYMBOL–N_2 GAS

SHADED SYMBOL–HELIUM GAS

a)EFFECT OF MASS FLOW

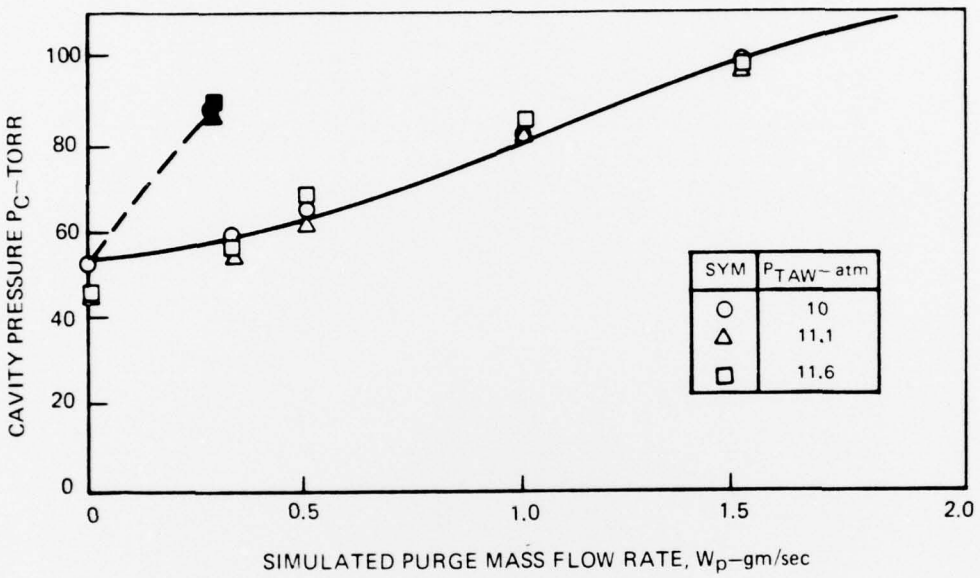

b)EFFECT OF VOLUMETRIC FLOW

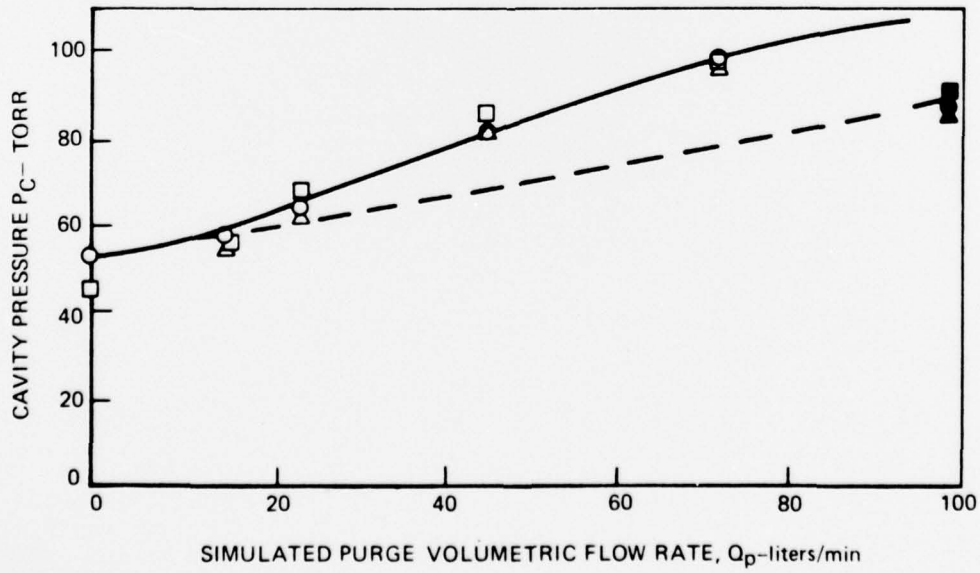

77–08–126–1

UNITED
TECHNOLOGIES
RESEARCH
CENTER

East Hartford, Connecticut 06108